We are IntechOpen, the world's leading publisher of Open Access books
Built by scientists, for scientists

4,800
Open access books available

122,000
International authors and editors

135M
Downloads

Our authors are among the

154
Countries delivered to

TOP 1%
most cited scientists

12.2%
Contributors from top 500 universities

WEB OF SCIENCE™

Selection of our books indexed in the Book Citation Index in Web of Science™ Core Collection (BKCI)

Interested in publishing with us?
Contact book.department@intechopen.com

Numbers displayed above are based on latest data collected.
For more information visit www.intechopen.com

Chapter 3

Resistivity Model of Frozen Soil and High-Density Resistivity Method for Exploration Discontinuous Permafrost

Wei Shan, Zhaoguang Hu, Ying Guo,
Chengcheng Zhang and Yao Liu

Additional information is available at the end of the chapter

http://dx.doi.org/10.5772/intechopen.68197

Abstract

In permafrost-degraded areas, "islands" of permafrost can be buried in the unfrozen soil. When permafrost is arranged in this discontinuous pattern, it is more difficult to analyze from an engineering or geological perspective. The degree of resistivity of unfrozen soil is determined by the dry density, temperature, moisture content, and pore water resistivity of the soil, as well as by the mineral composition, size, and cementing state of the soil particles. Part of the water in the soil pores experiences a phase change as the soil freezes, so permafrost has different resistivity than unfrozen soil. In this chapter, we explore the conduction characteristics of permafrost. First, we established a theoretical model to analyze the factors affecting the resistivity of permafrost. Next, we used an experimental study to analyze how unfrozen water content, initial moisture content, soil temperature, and dry density influence the resistivity of frozen soil. These experimental study results served to validate the rationality of the model of permafrost resistivity. To analyze differences in conductivity between underground media, we used a high-density resistivity (HDR) method, which infers the storage of underground geologic bodies with different resistivity based on the distribution of a conduction current under the electric field action. In this chapter, the WGMD-9 super HDR measurement system produced by the Chongqing Benteng Numerical Control Technique Research Institute was used to obtain the resistivity profile. The study region was the road area from Bei'an Expressway to Heihe Expressway in the permafrost degeneration area in Northeast China. A permafrost profile map was drawn based on data from engineering drilling and an analysis of factors that influence permafrost resistivity. The reliability of the permafrost profile map was verified by an analysis of temperature data taken at measured points at different depths of the soil profile.

Keywords: electrical resistivity, electrical resistivity model, high-density resistivity method, frozen soil

INTECH
open science | open minds

© 2017 The Author(s). Licensee InTech. This chapter is distributed under the terms of the Creative Commons Attribution License (http://creativecommons.org/licenses/by/3.0), which permits unrestricted use, distribution, and reproduction in any medium, provided the original work is properly cited. CC BY

1. Introduction

One of the innate attributes of a soil is the electrical resistivity. The dry density, water content, temperature, mineral composition, and structure of the soil determine the magnitude of the electrical resistivity. In a previous experimental study, the cementation factor was shown to be related to the shapes and cementation conditions of soil particles. A study by Wu et al. [1] preliminarily showed the factors that affected variation in the electrical resistivity of soils. The results showed that the electrical resistivity of the soil varied with soil type, mother rocks, soil texture, and soil salt content. Water content, the water-cement ratio, and the degree of saturation are well correlated with the electrical resistivity of a cement-soil mixture. Li et al. [2] assessed the relationship between the electrical resistivity of a saline soil and the salt content, water content, porosity, and degree of saturation. The results showed that the electrical resistivity of the saline soil decreased with increases in the water content, salt content, and the degree of saturation. Also, it increased with increasing porosity. Zha et al. [3] studied the effect of the particle composition of a soil on its electrical resistivity and showed that the electrical resistivity of the soil decreased with increases in the liquid limit or the plastic limit of the soil.

A calorimetric experiment on an undisturbed frozen soil sample was performed by Fortier et al. [4], and they also obtained the unfrozen water and ice contents in the sample. Fortier et al. [5] determined the electrical resistivity at the location near the sampling site and determined the relation between the electrical resistivity and the unfrozen water and ice contents using a linear regression analysis. A study of the electrical resistivity of frozen and petroleum-polluted soils was reported by Delaney et al. [6]. They found that the freezing conditions and petroleum pollution could both result in an increase in the electrical resistivity of the soil. Fu et al. [7] performed a study in which they monitored the electrical resistivity of silty clay obtained from the Beiluhe River on the Qinghai-Tibet Plateau during an entire uniaxial compression test that was carried out at different temperatures. They showed that the uniaxial compression strength of the frozen soil had a strong semi-logarithmic relationship with the initial electrical resistivity. The relationship between the electrical resistivity and the ice content of the frozen soil was obtained by Angelopoulos et al. [8] using the electrical resistivity method on the frozen soil from Parsons Lake in the Northwest Territories of Canada. The electrical resistivity method was also used to study the spatial distribution of the island-shaped permafrost layer along the Beian-Heihe highway. Discontinuities in the electrical resistivity at the upper and lower interfaces of the island-shaped permafrost layer were observed and permafrost layer showed significantly high resistance. Variation in the electrical resistivity of the areas without permafrost was relatively gentle with no discontinuities.

This study investigated the relationship between the electrical resistivity of a soil body and the water content, temperature, and dry density of the soil to thoroughly study the electrical conductive properties of frozen soils. We used mathematical deduction and a theoretical model for the electrical resistivity of frozen soils. Experiments were conducted on soil bodies with different water contents and dry densities at different temperatures. We also verified the reasonableness of the theoretical model for the electrical resistivity of frozen soils and provided a theoretical basis for exploring the distribution of underground shallow frozen soils with the electrical resistivity method.

In recent decades, geophysical analysis has become a common tool in studies that evaluate stratigraphic distribution. In situ geophysical techniques can directly or indirectly measure the physical parameters of rock and soil that are related to the lithological, hydrological, and geotechnical features of rocks and soils [9–11]. Compared with other ground detection technologies such as drilling, clinometry, and laboratory testing, these physical detection techniques are nondestructive and can integrate the information acquired over large soil volumes to overcome the point-scale limitations of standard geotechnical measurements. The high-density resistivity (HDR) method, an in situ geophysical technique, is increasingly being applied to geological surveys of landslides, permafrost, and so on [9, 12, 13].

By measuring the resistivity of subterranean rock and soil, the HDR method can provide relevant two-dimensional (2D) and three-dimensional (3D) images, which are used in geophysical exploration to gain solutions to shallow geologic problems [14–18]. The HDR method has already been applied in the arctic and alpine environments to identify the sliding surface of landslide and to detect the distribution of permafrost [17, 19–24]. As an effective detection method for permafrost exploration, the HDR method can determine the thickness and the upper and lower limits of permafrost, metrics that have been used in permafrost surveys since the late 1970s [10, 25–28]. However, all geophysical methods have their applicability, including regional limitations and reliability. The HDR method has not been effectively and extensively applied in analyses of permafrost in the high latitudes of Northeast China nor has geophysical exploration been applied in the permafrost areas in Lesser Khingan Mountains, China, to monitor the degradation process of permafrost.

In this chapter, the HDR measurement system was used to obtain the resistivity profile. The study region was the road area from Bei'an Expressway to Heihe Expressway in the permafrost degeneration area in Northeast China [29]. A permafrost profile map was drawn based on data from engineering drilling and an analysis of factors that influence permafrost resistivity. The reliability of the permafrost profile map was verified by an analysis of temperature data taken at measured points at different depths of the soil profile.

2. Establishing a model for the electrical resistivity of frozen soils

2.1. Models for the electrical resistivity of soils

An electrical resistivity model that is applicable to saturated non-cohesive soils and pure sandstones, assuming that the conductivity of solid particles is not considered, has been proposed [30]:

$$\rho = a\,\rho_w\, n^{-m} \tag{1}$$

where ρ is the electrical resistivity, ρ_w is the electrical resistivity of pore water, n is the porosity, a is an experimental parameter, and m is the cementation factor.

Archie [30] proposed an electrical resistivity model that related the electrical resistivity of a soil to the structure of the soil. It expanded the approaches for studying the microstructures of soils. This proposed model, however, only considered the effect of the electrical resistivity and

porosity of the pore water on the electrical resistivity of the soil. This means that the potential applications of the electrical resistivity proposed model are limited.

In later work, the electrical resistivity model proposed by Archie [30] was expanded to the following:

$$\rho = a\,\rho_w\, n^{-m}\, s_r^{\ -p} \tag{2}$$

where s_r is the degree of saturation and p is the saturation exponent.

In the expanded electrical resistivity model, the degree of saturation of the pore water is considered. The expanded model is therefore applicable to non-saturated pure sandstones and non-cohesive sand. The expanded model, however, ignores the effects of other factors on the electrical resistivity of a soil.

On the basis of experimental studies and considering the effect of the electrical double layers on the surfaces of soil particles on the electrical resistivity of the entire soil body, an electrical resistivity model that is applicable to non-saturated cohesive soils was proposed:

$$\rho = \frac{a\,\rho_w\, n^{-m}\, s_r^{\ 1-p}}{s_r + \rho_w BQ} \tag{3}$$

where B represents the electrical resistivity of the charge whose electrical property is opposite to that of the surface of the soil particle in the electrical double layer, Q is the cation exchange capacity per unit soil pore, and BQ is the electrical resistivity of the electrical double layer on the surface of the soil particle.

Wasman and Smits [31] proposed an electrical resistivity model that considered the effect of the electrical conductivity of soil particles on the electrical resistivity of the soil, which means that the electrical resistivity model proposed by Smits is applicable to non-saturated cohesive soils.

Beside pore water and soil particles, there is a third conductive propagation path for cohesive soils, that is, the series-coupled soil-water propagation path. Considering the previously mentioned three conductive propagation paths for cohesive soils, the following equation for the model for the electrical resistivity of non-saturated cohesive soils has been deduced:

$$\rho = \left[n\, s_r - F' \frac{\theta'}{1+\theta'} BQ + \frac{n\, s_r - F' \dfrac{\theta'}{1+\theta'}}{\rho_w} + \frac{F'(1+\theta')BQ}{1 + BQ\,\rho_w\,\theta'} \right]^{-1} \tag{4}$$

where F' is the conductive structure coefficient (the ratio of the width of the series-coupled soil-water path to the side length of the entire soil body) and θ' is the volumetric water content of the parallel-coupled soil-water part.

Zha et al. [32] proposed an electrical resistivity model that considered the effect of conductive paths and organically combined the electrical resistivity of a soil with factors such as porosity, degree of saturation, electrical resistivity of the pore water, soil structure, soil particle composition, and electrical double layers on the surfaces of soil particles. This thereby rendered the model for non-saturated cohesive soils more reasonable.

Equations describing the relation between electrical resistivity of a soil sample and the unfrozen water content as well as that between electrical resistivity of a soil sample and the ice content are the following [4, 5]:

$$\frac{\rho}{\rho_{uw_0}} = e^{-w_{uw}/w_{uw_0}} \tag{5}$$

$$\frac{\rho}{\rho_{i_0}} = \left(\frac{w_i}{w_{i_0}}\right)^a \tag{6}$$

where ρ is the electrical resistivity (Ωm), ρ is the unfrozen water content (%), w_i is the ice content (%), ρ_{uw_0} = 12,820 Ωm is the reference electrical resistivity for a reference unfrozen water content w_{uw_0} of 5%, ρ_{i_0} = 1316 Ωm is the reference electrical resistivity for a reference ice content w_{i_0} of 10%, and a = 1.73 is the exponent of the power law between the electrical resistivity and the ice content.

Fortier et al. [5] proposed a model for electrical resistivity that first considers the effect of the ice content of a soil. This model is therefore applicable not only to unfrozen soils but also to frozen soils. A frozen soil, however, is a complex multiphase body. Also, there are many factors that affect a frozen soil. This model proposed by Fortier et al. [5] only considers the effect of the ice content of a soil on the electrical resistivity of the soil. In addition, the preset reference electrical resistivity value has no generality.

Angelopoulos et al. [8] analyzed frozen soil from Parsons Lake in the Northwest Territories of Canada with the electrical resistivity method and the study results showed the relationship between the electrical resistivity of the frozen soil and the ice content. In the study, the electrical resistivity method was applied in frozen soil exploration and proved to be very useful. However, the results were quite discrete and poorly correlated. Also, the electrical resistivity method only considers the effect of the ice content on the electrical resistivity of the frozen soil and is therefore limited.

2.2. Establishing a model for the electrical resistivity of frozen soils

A fraction of the pore water of a soil goes through a phase change during the freezing process. The electrical resistivity characteristics of a frozen soil are therefore different from those of an unfrozen soil. In our study, we assumed that there are three conductive paths (soil particles, ice-water mixtures, and soil-ice-water mixtures, i.e., the gas propagation path is ignored) for a frozen soil, as was also assumed in the three-element electrical conduction model and the model for the electrical resistivity of unsaturated cohesive soils. We deduced the equation for the model for the electrical resistivity of frozen soils [33]:

$$\rho = \left[A \times \frac{a\,\theta^{-b}}{w} + \rho_d\left(B \times \frac{a\,\theta^{-b}}{w} + C\right) + D\right]^{-1} \tag{7}$$

where A–D represent coefficients that are related to the structural characteristics of the frozen soil and electrical resistivity of each component of the frozen soil, w is the water content of the frozen soil, $a\,\theta^{-b}$ is the unfrozen water content of the frozen soil, θ is the absolute value of the temperature of the frozen soil, and ρ_d is the dry density of the frozen soil.

2.3. Main factors influencing the electrical resistivity of a frozen soil

Four primary factors can affect the electrical resistivity of a frozen soil:

1. Soil type. Particle size, shape, and mineral composition show large differences between the solid particles of different soil types. The mineral composition plays an important role in

the conductive path of soil particles. This results in differences in the electrical resistivity for different soil types.

2. Structural characteristics of the soil. The structural characteristics of the ice-water mixture and the shapes and orientations of soil particles are factors that determine the structural characteristics of the soil.

3. Pore water affects the electrical resistivity of a frozen soil based on the water content and the number and types of ions in the pore water. The initial water content and the unfrozen water content affect the electrical resistivity of a frozen soil. The unfrozen water content depends on the temperature and initial water content. The conductive properties of a soil body are affected by the types and number of ions in the pore water. The salt content (for soils that contain salt) determined the types and number of ions. When a soil body contains salt, soluble minerals are dissolved in the pore water and they exist in the form of ions. The migration of positive and negative ions occurs under the effect of an external electrical field. The concentrations of the ions in the pore water and the charge number that each ion carries determine the conductive properties of pore water.

4. Temperature changes the activity of ions and the unfrozen water content. The water in a soil body solidifies and forms ice when the temperature is less than 0°C. When this happens, the unfrozen water content of the soil body decreases and there is a relatively large change in the electrical resistivity of the frozen soil with the water changing from a liquid state to a solid state.

Frozen soil consists of soil particles, ice-water mixtures, and gas. We know from Eq. (7) that factors that affect the electrical resistivity of a frozen soil include the electrical resistivity and the structure coefficient, dry density, water content, content of each component, and temperature. Eq. (7) shows that when the initial water content of the same frozen sample is fixed, the electrical resistivity of the frozen soil is inversely proportional to the unfrozen water content of the soil body. The unfrozen water content varies with changes in the initial water content in frozen samples with different initial water contents. Also, the electrical resistivity of the frozen soil exhibits a complex temperature-related functional relationship with the initial water content. The electrical resistivity of a frozen soil has an exponential relationship with the temperature of the soil body. Also, it is inversely proportional to the dry density of the soil body.

3. Experimental verification of the model for the electrical resistivity of frozen soils

3.1. Electrical resistivity measurement principle

Figure 1 shows the principle diagram of the electrical circuit of the device used to measure the electrical resistivity. To reduce the disturbance of the frozen soil samples, a two-electrode electrical resistivity measurement system was used for electrical resistivity measurements. The electrical resistivity of a soil body is calculated using the following equation:

http://dx.doi.org/10.5772/intechopen.68197

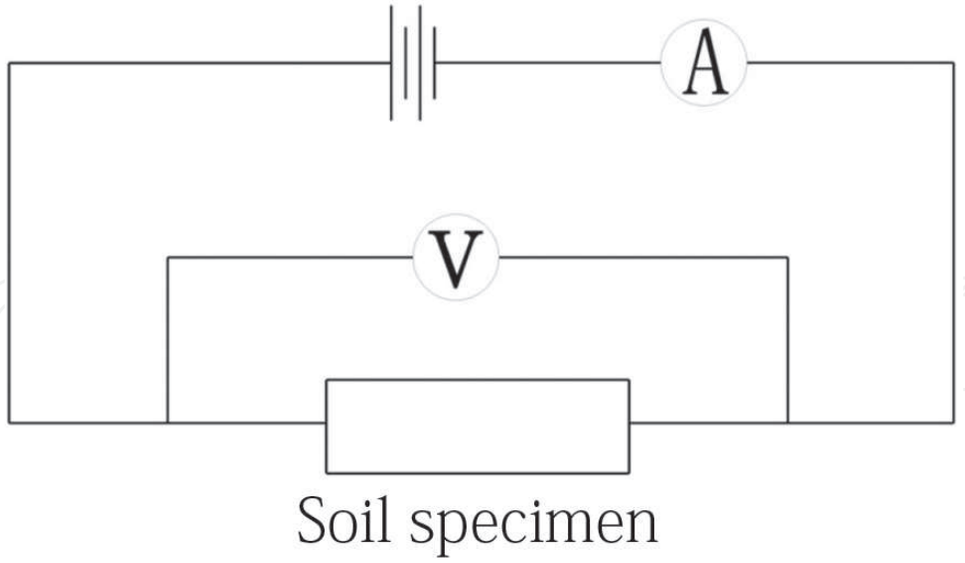

Figure 1. Schematic diagram of the electrical resistivity measurement circuit.

$$\rho = \frac{\pi U D^2}{4IL} \tag{8}$$

where ρ is the electrical resistivity (Ωm), U is the voltage between the two ends of the soil sample (V), I is the current that passes through the soil sample (A), and L is the length of the soil sample (m).

3.2. Experimental materials

The experimental soil sample was silty clay. The original soil samples were sieved, air-dried, and ground for use in the experiment. A 2-mm sieve was used and the soil particles with sizes less than 2 mm were retained and used as the experimental soil sample. The cumulative particle size distribution curve of the experimental soil sample is shown in **Figure 2**. The basic physical properties of the experimental soil sample are shown in **Table 1**. The experimental soil sample had a maximum dry density of 1.89 g·cm^{-3} and the corresponding optimum water content was 13.4%.

3.3. Experimental scheme and steps

The experimental soil was fabricated into a cylindrical specimen with a dry density of 1.52 g·cm^{-3}, an initial volumetric water content of 13.68%, and dimensions ($h \times \phi$) of 300 mm × 158 mm at 24°C to study the variations in the unfrozen water content and the electrical resistivity of the soil body with temperature during the freezing process. Also, the specimen was sealed and then placed in an insulating sleeve with an internal diameter of 160 mm. A water content sensor and a temperature sensor were embedded in the specimen (the temperature sensor had a measurement range of −40 to 50°C and a measurement accuracy of 0.01°C; the water content sensor had a measurement accuracy of 0.01). Copper electrodes with a thickness of 0.5 mm and a purity of 99.5% were placed at each end of the specimen. Subsequently, the specimen was moved outside and allowed to solidify gradually at −24 to −32°C. A LOGGER 3.0 experimental system

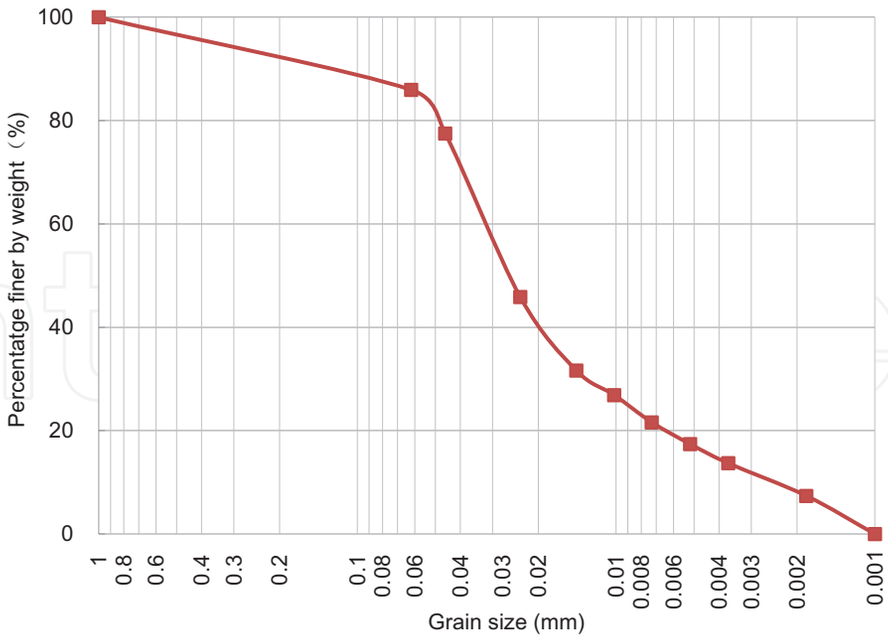

Figure 2. Particle size distribution curve of the soil sample.

Name of the soil sample	Natural water content (w/%)	Optimum water content (w_{op}/%)	Maximum dry density (ϱ_d/g·cm^{-3})	Plastic limit (W_P)	Liquid limit (W_L)	Plasticity index (I_P)	Specific weight (*Gs*)
Silty clay	28.3	13.4	1.89	17.93	33.06	15.13	2.71

Table 1. Basic physical property indexes of the experimental soil sample.

(Beijing Huizenong Tech. Co., Limited is located in Haidian District, Beijing City, China) was employed to automatically acquire the volumetric water content and temperature of the soil body at a 5-minute interval during the freezing process. The electrical resistivity of the specimen was simultaneously measured (**Figure 3**). The variation curves of the electrical resistivity of the soil body and unfrozen water content of the soil body with temperature were obtained after calculating and processing the acquired data (**Figure 5**). The soil water content sensor-working principle was as follows: the standing wave ratio principle was used to measure the volumetric water content, that is, the variation of the dielectric constant (ε) of the soil body is measured and then transformed to the volumetric water content (θ_v) using the Topp equation [34]:

$$\theta_v = -5.3 \times 10^{-2} + 2.92 \times 10^{-2}\,\varepsilon - 5.5 \times 10^{-4}\,\varepsilon^2 + 4.3 \times 10^{-6}\,\varepsilon^3 \tag{9}$$

where θ_v is the volumetric water content and ε is the dielectric constant.

The dry density, temperature, and required soil and water masses were calculated according to the water content and dry density during the experiment to study the relationships between the electrical resistivity of the frozen soil and the initial water content. Water and soil were mixed homogeneously and sealed in a double-layer plastic bag for 12 h to allow the soil sample and water to mix homogeneously. The soil-water mixture was compacted layer by layer into specimens with dimensions ($h \times \phi$) of 80 mm × 39.1 mm according to the different dry density

http://dx.doi.org/10.5772/intechopen.68197

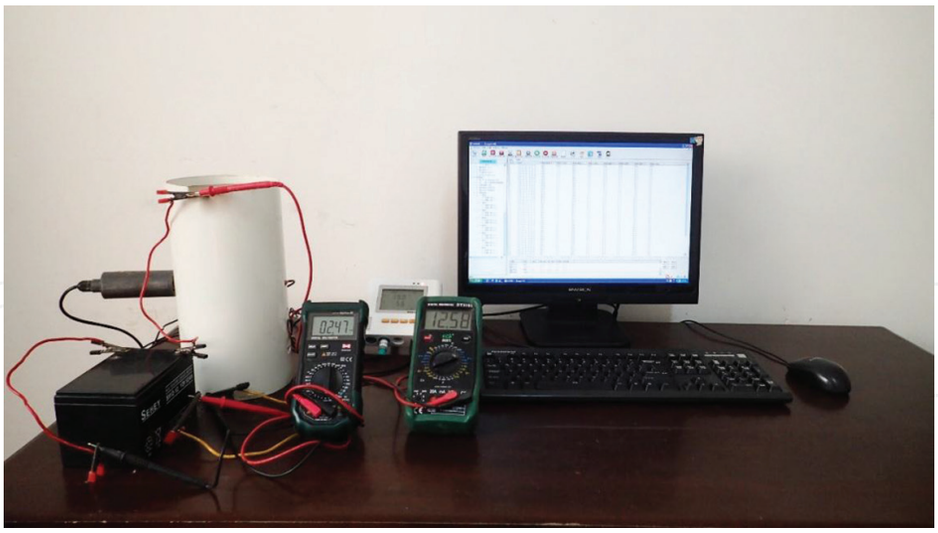

Figure 3. The LOGGER 3.0 system and the electrical resistivity measurement device.

requirements. Each soil specimen was sealed in a rubber membrane to prevent the water content of each soil specimen from changing during the freezing process. The environment of the experiment was a closed system and the experimental soil specimens were placed in a DX-200 low-temperature test chamber. The temperature of the low-temperature test chamber was set to the preset temperature during the experiment and was then maintained for 24 h. Then, the experimental soil specimens were placed in a low-temperature test chamber for 72 h. Three soil specimens were controlled in parallel under each set of conditions with consideration for the discreteness of the soil specimens. A copper electrode was placed at each end of each specimen after the freezing process was completed. Next, each specimen was placed in the device shown in **Figure 4** to measure its electrical resistivity. A DY2101 digital multi-meter was used to measure the voltage of each specimen. The measurement accuracy for the direct current voltage was ±0.5%. A MS8265 digital multi-meter was used to measure the current. The measurement

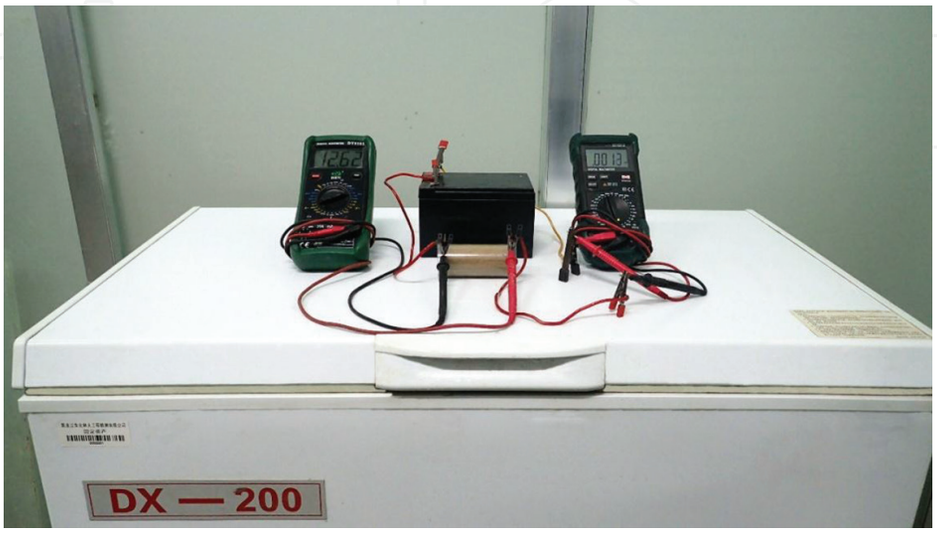

Figure 4. Photograph of the electrical resistivity measurement device.

accuracy for the current was ±0.5%. A DX-200 low-temperature test chamber that had the same temperature as the specimen was used to measure the electrical resistivity of each specimen.

Through manipulating the three factors—the water content (including the unfrozen and initial water content), the temperature, and the dry density—the values of electrical resistivity of the frozen soil for different water contents, temperatures, and dry density conditions were obtained. The curves of the relationships between the electrical resistivity of the frozen soil and different factors are plotted in **Figures 5–13**.

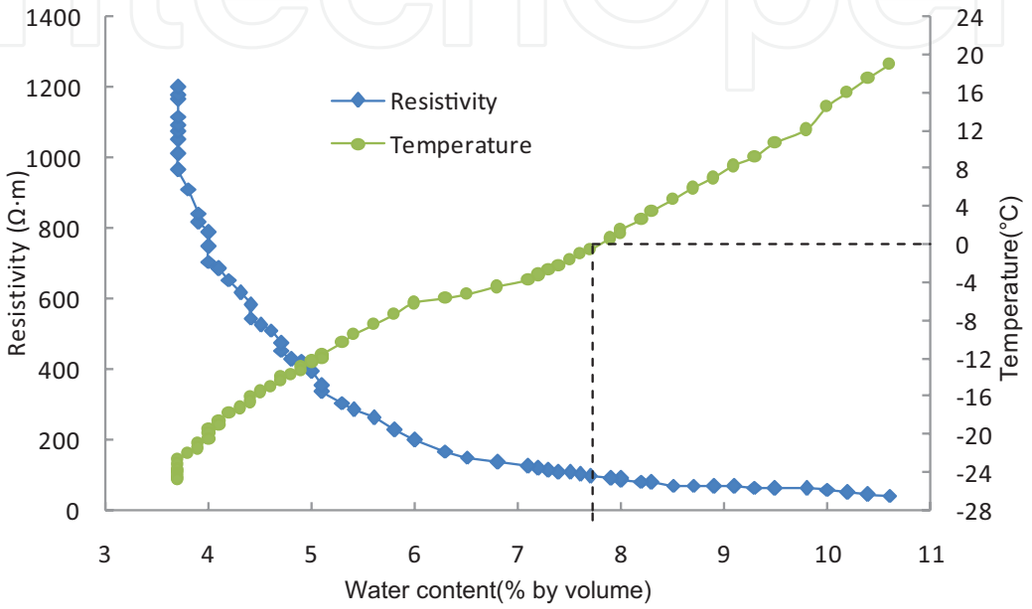

Figure 5. Variation curves of the electrical resistivity of the soil body and unfrozen water content of the soil body with temperature during the freezing process (ρ_d = 1.52 g·cm^{-3}; the initial water content was 13.68%).

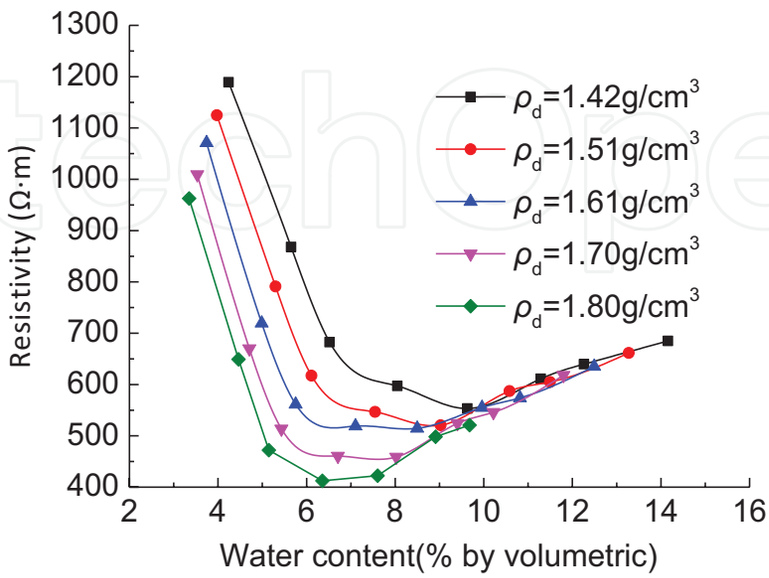

Figure 6. Curves of the relationship between the electrical resistivity of the frozen soil and water content under different dry density conditions (T = −17°C).

http://dx.doi.org/10.5772/intechopen.68197

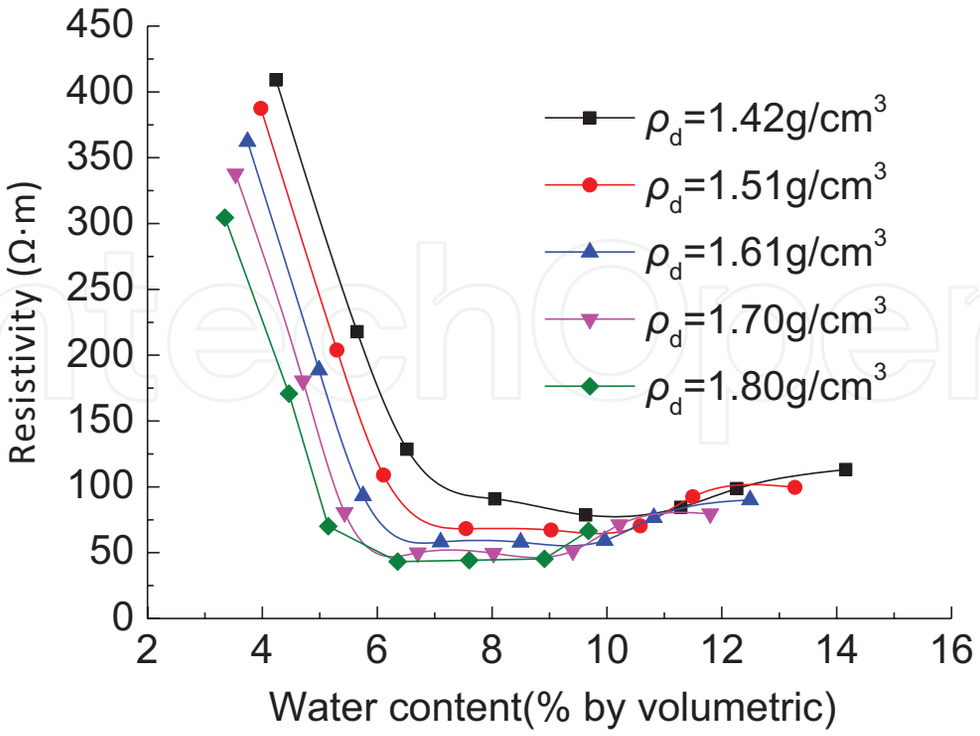

Figure 7. Curves of the relationship between the electrical resistivity of the frozen soil and water content under different dry density conditions (T = −3°C).

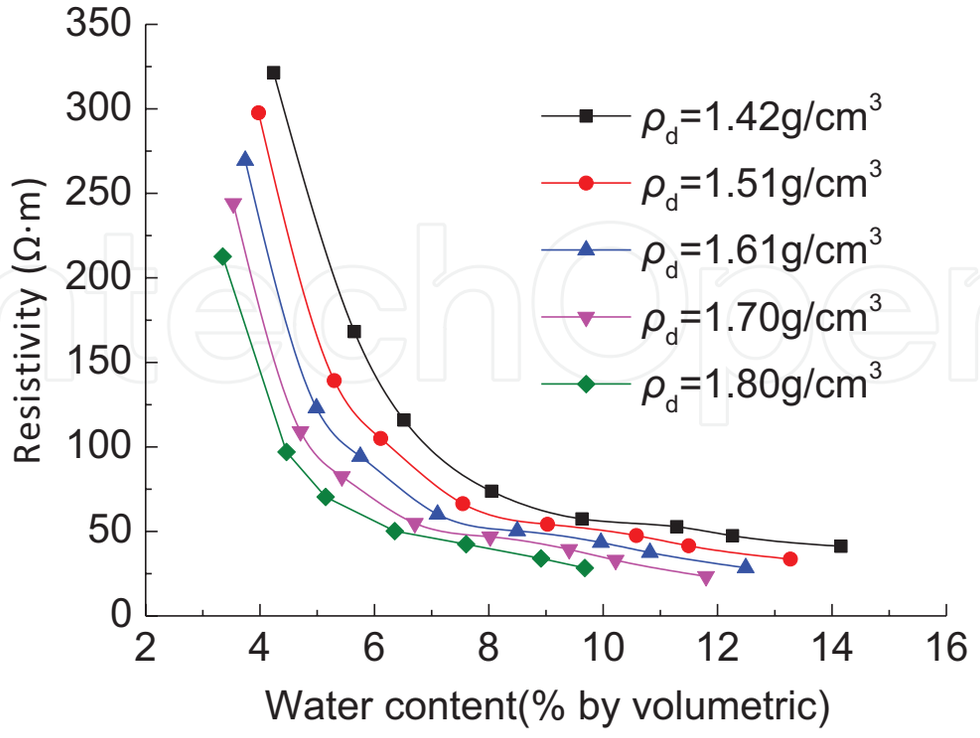

Figure 8. Curves of the relationship between the electrical resistivity of the frozen soil and water content under different dry density conditions (T = 3°C).

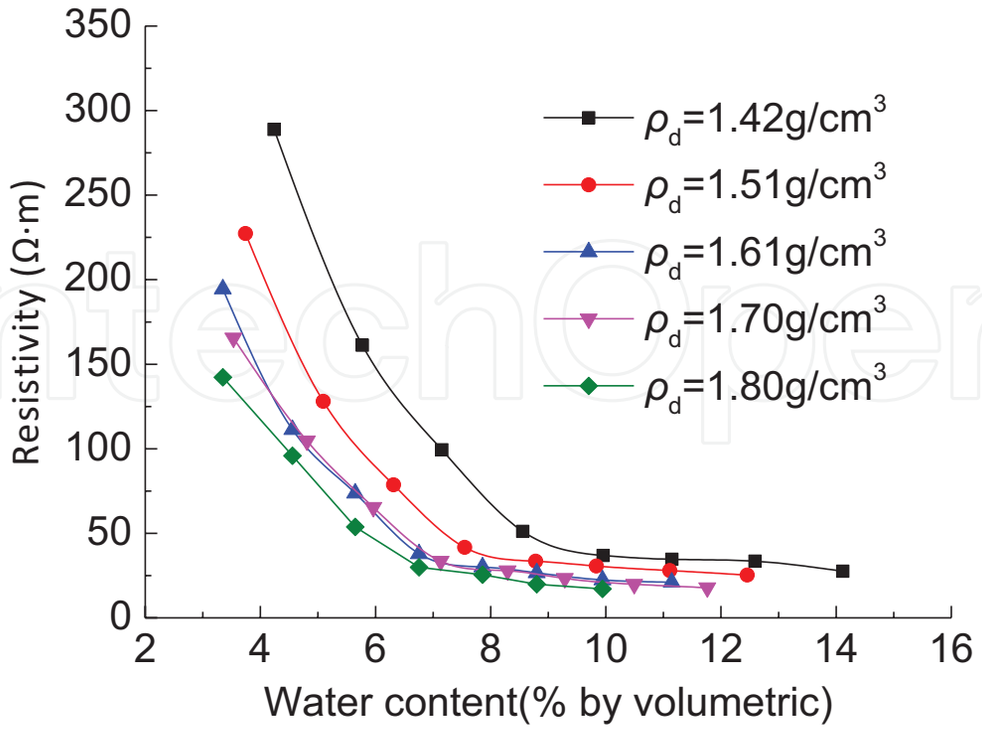

Figure 9. Curves of the relationship between the electrical resistivity of the frozen soil and water content under different dry density conditions (T = 17°C).

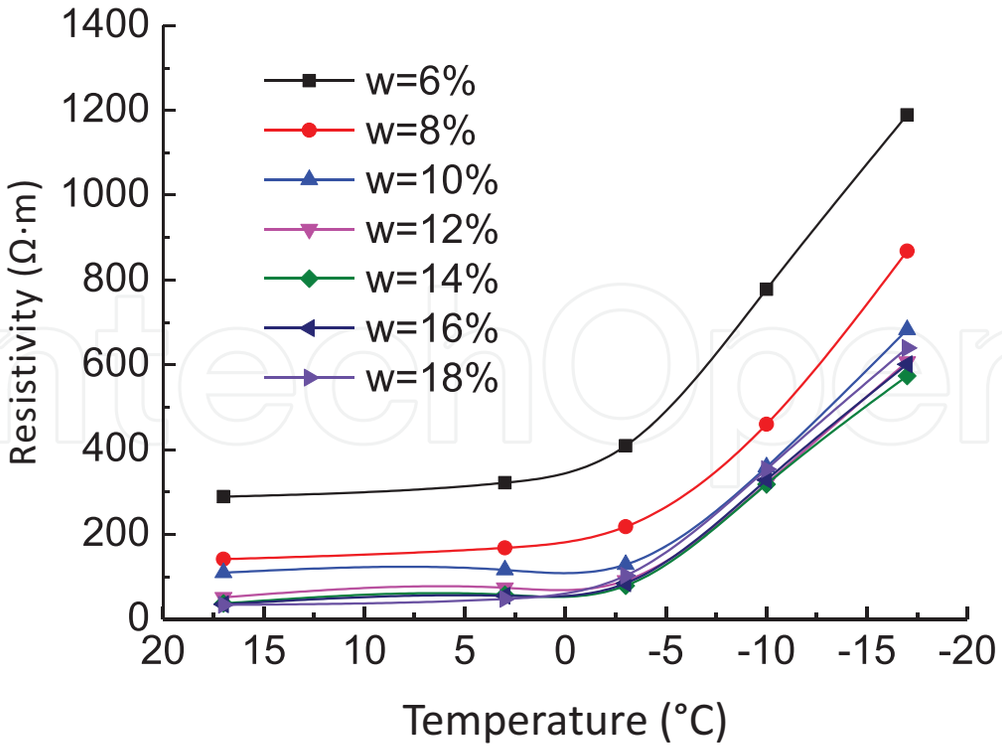

Figure 10. Curves of the relationship between the electrical resistivity and temperature under different water content conditions (ρ_d = 1.42 g·cm^{-3}).

http://dx.doi.org/10.5772/intechopen.68197

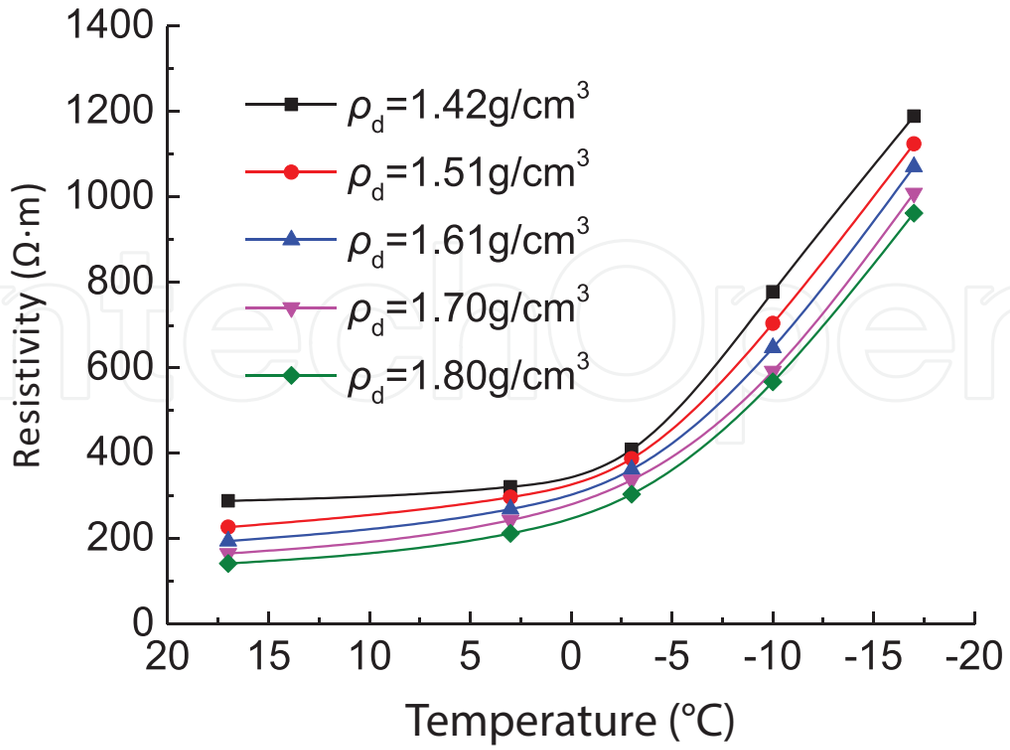

Figure 11. Curves of the relationship between the electrical resistivity and temperature under different dry density conditions (w = 6%).

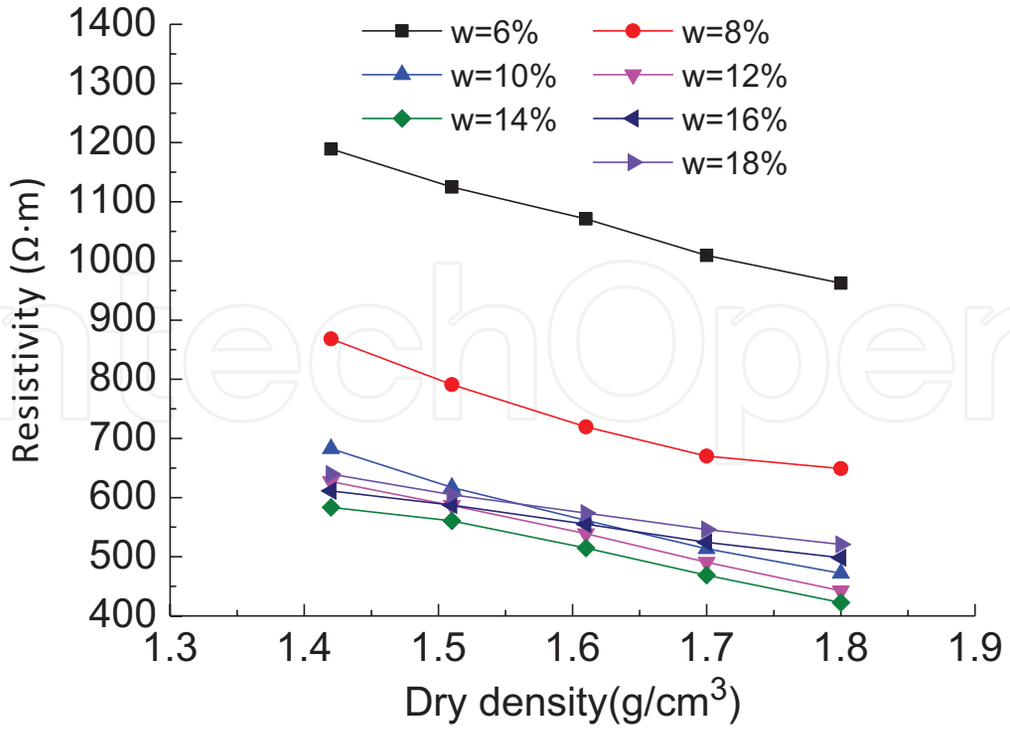

Figure 12. Curves of the relationship between the electrical resistivity and dry density of the frozen soil under different water content conditions (T = −17°C).

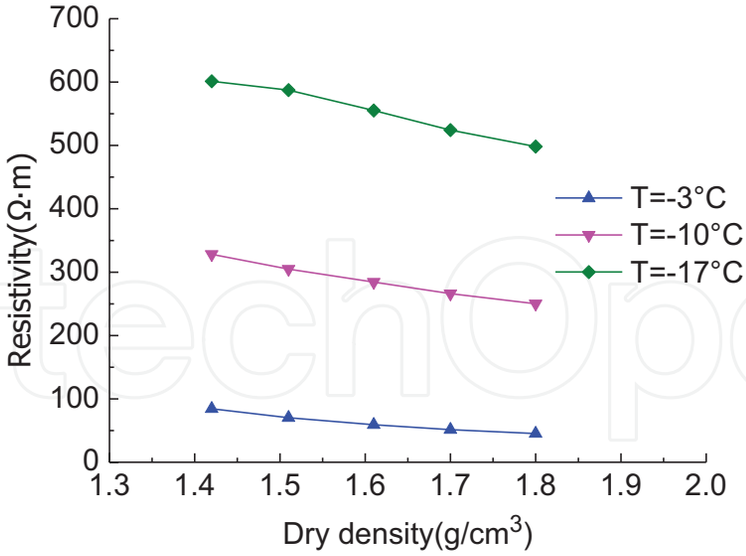

Figure 13. Curves of the relationship between the electrical resistivity and dry density of the frozen soil under different temperature conditions (w = 12%).

4. Analysis of the experimental results

4.1. Effects of the water content

The curve of the relationship between the electrical resistivity of the soil body and the water content, along with the curve of the relationship between the temperature and the water content, is shown in **Figure 5**. Dotted lines mark the volumetric water content of the soil body and the electrical resistivity of the soil body when T = 0°C.

The soil body started to solidify as the temperature was decreased when the temperature was less than 0°C. Also, some of the water in the soil body underwent a phase change. The volumetric water content approximated the unfrozen water content of the frozen soil. The curve of the relationship between the water content and the electrical resistivity of the frozen soil on the left side of the vertical dotted line approximates the relationship between the electrical resistivity of the unfrozen water content and the frozen soil. **Figure 5** shows the experimental curves indicating that the electrical resistivity of the frozen soil decreased with increases in the unfrozen water content of the frozen soil. The relationship between the electrical resistivity of the frozen soil and the unfrozen water content obtained through fitting was the following:

$$\rho = \frac{6172}{\theta_v} - 739, \quad R^2 = 0.910 \tag{10}$$

From Eq. (7), we know that in the model, the electrical resistivity of the frozen soil is inversely proportional to the unfrozen water content, which depends on the temperature; this relationship is consistent with the experiment results, thus verifying the reasonableness of the relationship between the unfrozen water content and the electrical resistivity in the proposed model for the electrical resistivity of frozen soils.

Figures 6–9 show the curves of the relationship between the electrical resistivity of each frozen soil specimen and the initial water content under different dry density conditions (the unfrozen soil [T = 3°C, T = 17°C] is used as the reference); the volumetric water contents shown in **Figures 6–9** were converted from the mass water contents. It can be observed from the experimental curves that the electrical resistivity of the frozen soil first rapidly decreased and then slowly decreased with increasing initial water content of the soil body, and the electrical resistivity of the frozen soil reached its minimum value near the optimum water content. When the initial water content was greater than the optimum water content, the effect of the dry density on the electrical resistivity of the frozen soil gradually decreased. The effect of the variation of the water content on the electrical resistivity of the frozen soil increased with decreasing temperature because of the following reasons: the effect of the variation of the water content on the electrical resistivity of the frozen soil decreased with the decreasing temperature, with increasing water content (i.e., increasing ice content of the frozen soil); the electrical resistivity of ice was greater than that of unfrozen water, thereby resulting in more rapid changes in the electrical resistivity of the frozen soil.

4.2. Effects of the temperature

The variation curves of the electrical resistivity of the frozen soil with temperature under different water content conditions (ρ_d = 1.42 g·cm^{-3}) and the variation curves of the electrical resistivity of the frozen soil with temperature under different dry density conditions (w = 6%), respectively, are shown in **Figures 10** and **11**. The unfrozen soil was used for comparison (T = 3°C, T = 17°C). The curves show that the electrical resistivity of the frozen soil increased with decreasing temperatures. We know that, in the proposed model (Eq. (7)), when there is a change in the dry density of the frozen soil or the water content of the frozen soil, the electrical resistivity of the frozen (ρ) is exponentially related to the temperature of the frozen soil (θ; the related parameters are different). This dependence is completely consistent with the experimental results. Thus, the reasonableness of the relation between the temperature and the electrical resistivity in the model for the electrical resistivity of frozen soils was verified. The decrease in temperatures resulted in a decrease in the unfrozen water content of the frozen soil, which then resulted in an increase in the electrical resistivity of the frozen soil. Since the soil sample still contained a large amount of unfrozen water at −3°C, there was no significant change in the electrical resistivity of the frozen soil when the temperature of the soil decreased from 17 to −3°C. Therefore, this resulted in a significant decrease in the electrical resistivity of the soil sample. The effect of temperature on the electrical resistivity of the frozen soil decreased with increases in the water content.

4.3. Effects of the dry density

The variation curves of the electrical resistivity of the frozen soil with the dry density under different initial water content conditions (T = −17°C) and the variation curves of the electrical resistivity of the frozen soil with the dry density under different temperatures (w = 12%) are shown in **Figures 12** and **13**, respectively. The experimental curves show that the electrical resistivity of the frozen soil decreased with increasing dry density in all cases. In the proposed model (Eq. (7)), it is known that when there is a change in the initial

water content of the frozen soil or the temperature of the frozen soil, the electrical resistivity of the frozen soil (ρ) is inversely proportional to the dry density of the frozen soil (ρ_d; the related parameters in the relationships are different). This dependence was consistent with the experimental results. This verified the reasonableness of the relationship between the dry density and the electrical resistivity of the frozen soil in the proposed model for the electrical resistivity of frozen soils. The porosity of the soil sample decreased when the dry density of the soil sample increased. The unfrozen water content of the frozen soil was the same under the same initial water content and temperature conditions. The increase in the dry density of the frozen soil resulted in a decrease in the electrical resistivity. This was due to the increase in the number of connections between soil particles. The effect of the variation of the dry density on the electrical resistivity of the frozen soil decreased with increases in the water content.

4.4. Effects of the freezing mode and salt content

During the freezing process of a soil body, water migration always occurs. The formation of various cryogenic structures, ice lenses, and different freezing temperatures and modes results in different freezing rates and ice nucleation modes of the water in a soil. There are different impacts on the electrical resistivity of the frozen with different ice nucleation modes. In the present study, however, the specimens were only frozen unidirectionally in a closed system.

The salt contents of the soil body are also primary factors that affect the electrical resistivity of the frozen soil [35]. However, the salt contents of the soil body were not considered in the present study. Further studies are necessary to investigate the relationship between the electrical resistivity of a frozen soil and the salt content of the frozen soil.

5. Application examples of resistivity

5.1. Study area

The K161 road section of Bei'an-Heihe Expressway was selected as the study area. This area intersects the northwest section of Lesser Khingan Mountains at the junction of Sunwu County and Heihe City, China's Bei'an-Heihe Expressway between 127°17′31″—127°21′24″– east longitude and 49°30′57″—49°41′50″– north latitude (**Figure 14**). The study area has a continental monsoon climate; a short spring quickly moves into a warm and rainy summer, followed by a short autumn accompanied by a rapid drop in temperature, and a long and cold winter. The annual average temperature is 0.6°C, the lowest temperature is −48.1°C, and the highest is 35.2°C. Soil in the study area begins to freeze at the end of October each year, and extends to a maximum seasonal freezing depth of between 2.26 and 2.67 m. The frozen soil on the ground surface begins to melt in April, and the melting stage lasts from April to September. In dry regions, all the frozen soils will melt by about early July, whereas in swampy regions, the thick layers of peat and humus will not melt until October. Seasonal frozen soil is well developed in the study area and "islands" of permafrost are also distributed in some gully areas.

http://dx.doi.org/10.5772/intechopen.68197

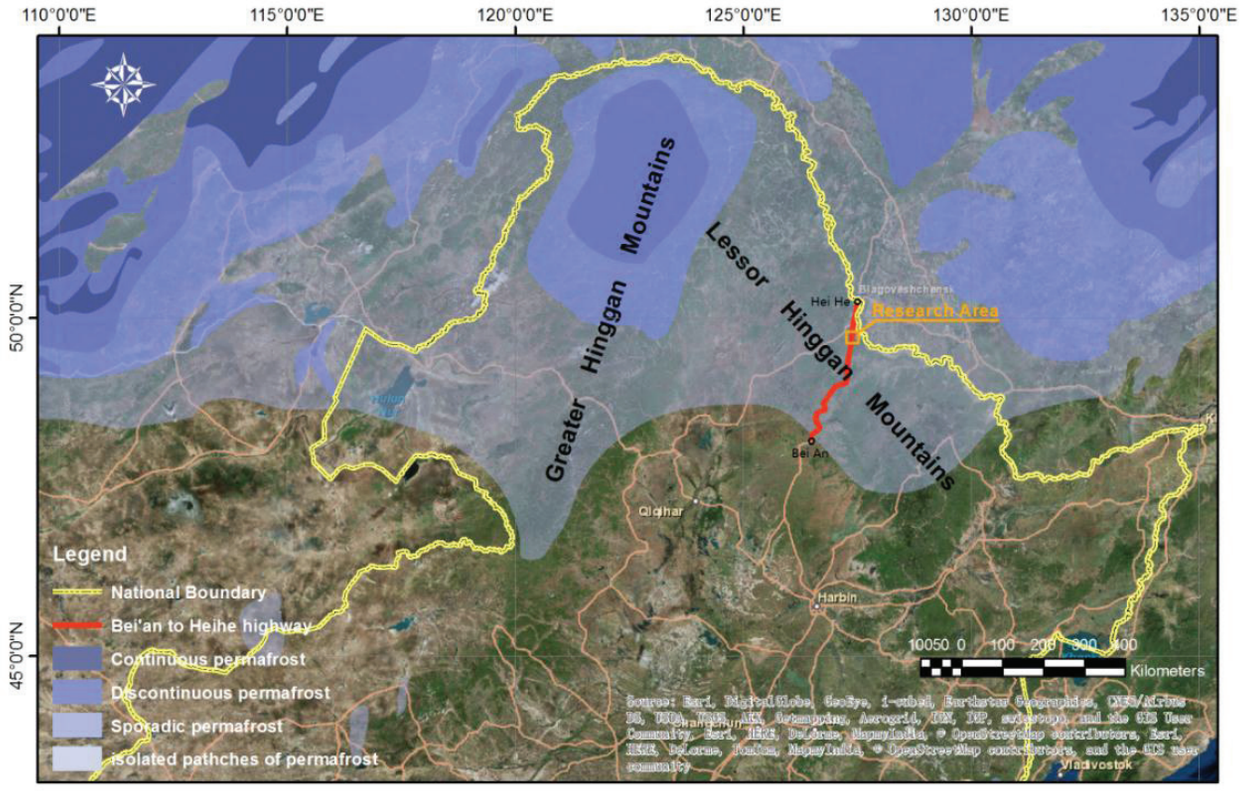

Figure 14. The permafrost distribution map at high latitudes in Northeast China and geographical location of the study area (data courtesy of the University of Zurich).

The area is located in the southern margin of China's high-latitude permafrost region, where the island permafrost is sedimentary residue of the ancient glacier and is currently in a degradation stage. The Bei'an-Heihe Expressway is an expressway widened and expanded based on the original Heihe-Bei'an Second-Class Highway, which was built in 1997 and completed and opened to traffic in 2000. As indicated by the Research Report on Engineering Geological Investigation and Evaluation of Permafrost in the Heihe-Bei'an Section of the Heihe-Dalian Highway, there are 17 road sections containing island permafrost along the Heihe-Bei'an Highway in 2000. In 2009, an engineering geological investigation of the whole area along the Heihe-Bei'an Highway showed that there were only seven road sections containing island permafrost and that permafrost in the other 10 road sections had disappeared. Compared with the investigation results in 2009, the permafrost layers in the seven road sections are now even more reduced in length and thickness, and the lower limits of permafrost are no longer as deep. The temperature of the study area has been increasing in recent decades and the ground temperature has increased as well. If the ground temperature of the study area continues to rise in the coming decades, the permafrost in this area will continue to degrade.

The tectonic structure of the study area is located in the new Wuyun-Jieya Fault Depression Belt, with the Handaqi Fold Belt on the north and the Shuhe uplifted belt on the south. The exposure strata (from old to new) include the Nenjiang Formation of Upper Cretaceous, the Sunwu Formation of Tertiary System, and the Modern River Alluvium of the Holocene

Series of Quaternary System. Permafrost is mainly distributed in the Modern River Alluvium of the Holocene Series and the Nenjiang Formation of the Upper Cretaceous. Water inputs in the study area mainly from the surface water, ground water, and underground ice.

5.2. Geological survey

The island permafrost in the study area is developed in the low-lying marshlands where there is surface water, overgrown grasses, and thickly accumulated turf and peat. The fundamental reason for the maintenance and preservation of degraded permafrost is that the amount of heat in permafrost is insufficient to melt permafrost in the short term. These marshes provide abundant material resources for evaporation in the warm season, which dissipates a large amount of heat in the atmosphere in the form of latent heat. Additionally, the dense grasses and the rich turf and peat under the soil surface are good thermal insulation materials that prevent the heat absorbed on the surface from being spread to the deep sections of the soil, preventing the temperature of permafrost from rising. In the freezing period, water in the wetland is turned into ice, increasing the thermal conductivity of the soil layer. However, during this freezing period the soil releases heat into the atmosphere. Enhanced thermal conductivity further increases the amount of heat released by the soil layer, which can also lower the temperature of the permafrost. These characteristics of wetlands directly affect the long-term preservation of island permafrost in the permafrost areas.

In this study, we investigated the engineering geological and hydrogeological conditions of the study area and measured its upper and lower limits of permafrost. In July 2009, five drill holes were arranged at the left slope toe, left shoulder, central separator, right shoulder, and right slope toe of the road (drilling locations are shown in **Figure 15**). An engineering geological section map of the study section was drawn according to the drilling results (**Figure 15**).

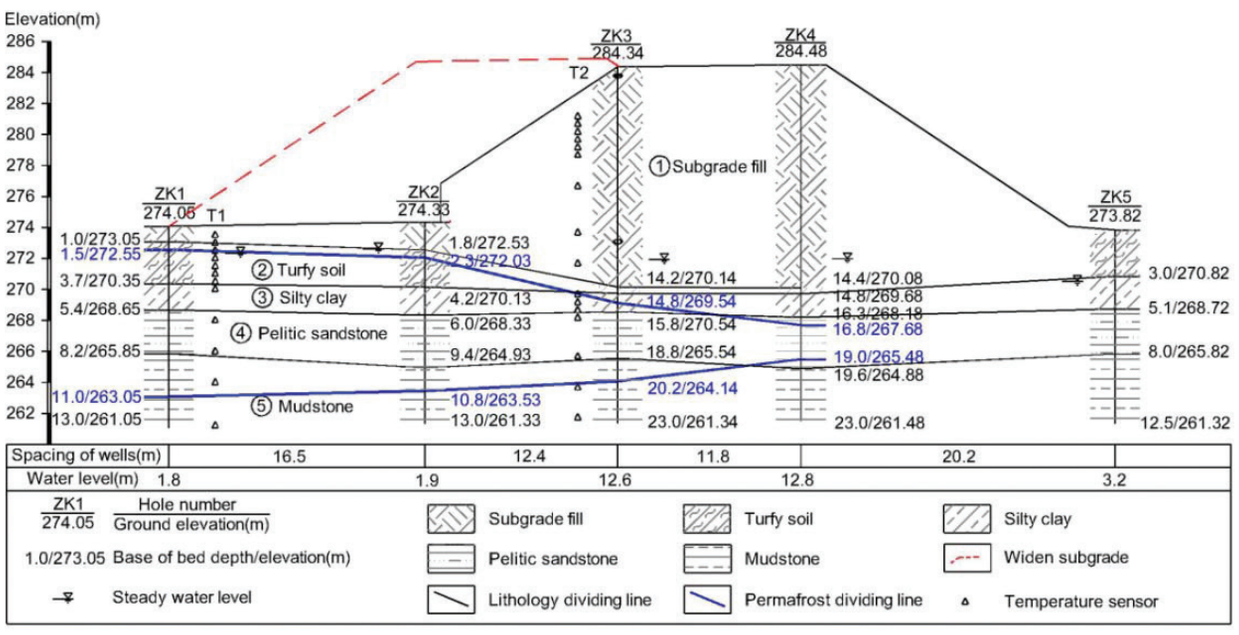

Figure 15. The geological section map.

http://dx.doi.org/10.5772/intechopen.68197

Soils and rocks in the control area include Quaternary loose soils, Cretaceous sandstone, and mudstone. The subgrade fill is mainly yellow pebbly sandstone which is slightly dense and permeable. The turf contains incompletely decomposed grassroots, with a layered and patchy frozen soil structure that is brownish black, saturated, and soft plastic. The silty clay layer is black, wet, hard plastic, and glossy, with relatively large dry strength and toughness, and a layered and patchy frozen soil structure. The argillaceous sandstone contains partial fine sandstone lens, with weak cementation, pelitic texture, layered structure, and a micro-layer, and layered frozen soil structure that is gray-black, wet, and hard plastic. The mudstone layer is gray-black, wet, and hard plastic, with weak cementation, pelitic texture, layered structure, and a layered frozen soil structure.

The ground water was comparatively deep at a subgrade depth of 12.4–12.5 m and relatively shallow at the slope toe at a depth of 1.7 m. The upper limit of permafrost was 15.8–16.8 m and the lower limit was 19.0–20.3 m at the old subgrade and the permafrost thickness was less than 5.0 m. The upper limit of permafrost in the original ground was 1.5–2.3 m, the lower limit was 9.2–10.8 m, and the permafrost thickness was 7.7–8.5 m. Affected by the old road filling, the permafrost beneath the old subgrade had degraded significantly and there was no permafrost at the right slope toe.

To explore the temperature change of permafrost below the subgrade during construction and operation of roads, we used the SUR-3 soil temperature sensor produced by the Beijing Huizenong Technology Co., Ltd. This drilling machine has a measurement range of −40 to 120°C. The machine was used to drill holes at two test points, T1 and T2, and soil temperature sensors were embedded in these drilled holes. T1 and T2 were close to ZK1 and ZK3, respectively. **Figure 15** shows the layout of the temperature sensors.

5.3. The HDR method

The HDR method was used to conduct a geophysical exploration of the K161 road section. Three HDR measuring lines were arranged in the K161 road section: I–I′, II–II′, and III–III′ (**Figure 16**).

The instrument used in this study was the WGMD-9 super HDR measurement system produced by the Chongqing Benteng Numerical Control Technique Research Institute. With the super WDA-1 digital-DC electrical prospecting apparatus as the measurement and control host, the system realizes the centralized 2D measurement of high-density resistivity by matching the WDZJ-4 multi-channel switcher and centralized high-density cables and electrodes. The 2DRES HDR method was used to invert the field data. The inversion model was based on the smooth-constrained least-squares method. In brief, this method constantly adjusts the resistivity of the model via model corrections to reduce the difference between the calculated apparent resistivity and the measured apparent resistivity, and it describes the fitting degree between the two using the mean square error. The least-squares method based on smooth constraint is an approach that is widely used because it can be adapted to different types of data and models, data inversion is fast and less affected by noise, the method has high sensitivity to deep units, and there are only a small number of iterations.

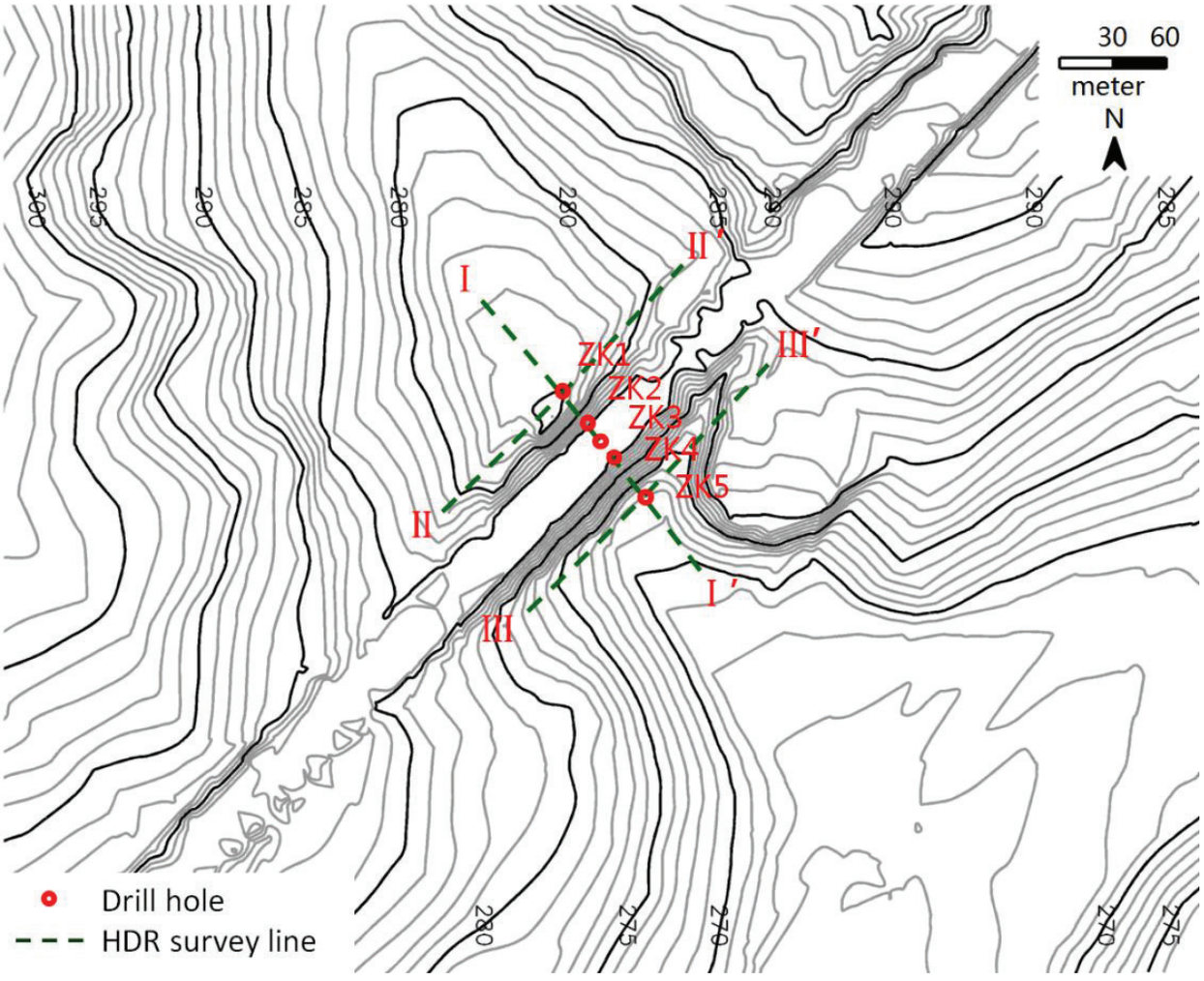

Figure 16. The arrangement plan of the HDR measuring lines in the K161 road section. HDR measuring line: (1) located on the cross section of K161+440, the I–I′ measuring line is perpendicular to the road direction; the starting point of the measuring line is 60 m away from the left slope toe of the road, and the line passes ZK1, ZK2, ZK3, ZK4, and ZK5 in succession; the end of the measuring line is located 60 m outside the right slope toe of the road. (2) Located at the left slope toe of the road, the II–II′ measuring line is parallel to the road direction, with ZK1 as the midpoint, with the starting point in the southwest and the end point in the northeast. (3) Located at the right slope toe of the road, the III–III′ measuring line is parallel to the road direction, with ZK5 as the midpoint, with starting point in the southwest and the end point in the northeast. All the three HDR measuring lines are 177 m long. The Wenner arrangement method was used to arrange the measuring lines, with the electrode spacing at 3.0 m and the limit surrounding at 30 m.

5.4. Analysis and discussion on the HDR method and ground temperature data

5.4.1. Ground temperature data

A contour map showing the variation of different ground temperatures and depths with time was drawn according to the ground temperature data of rock and soil monitored by the temperature sensor at T1 (**Figure 17** shows the variation of the upper and lower limits of the permafrost at T1 over time). In July 2009, the upper limit of the permafrost was 272.7 m, the lower limit was 263.0 m, and the thickness was 9.7 m. When ground temperature monitoring began in September 2009, the upper limit of the permafrost was 272.5 m, the lower limit was 263.2 m, the thickness was 9.3 m, and the lowest temperature of the permafrost was −1.2°C

http://dx.doi.org/10.5772/intechopen.68197

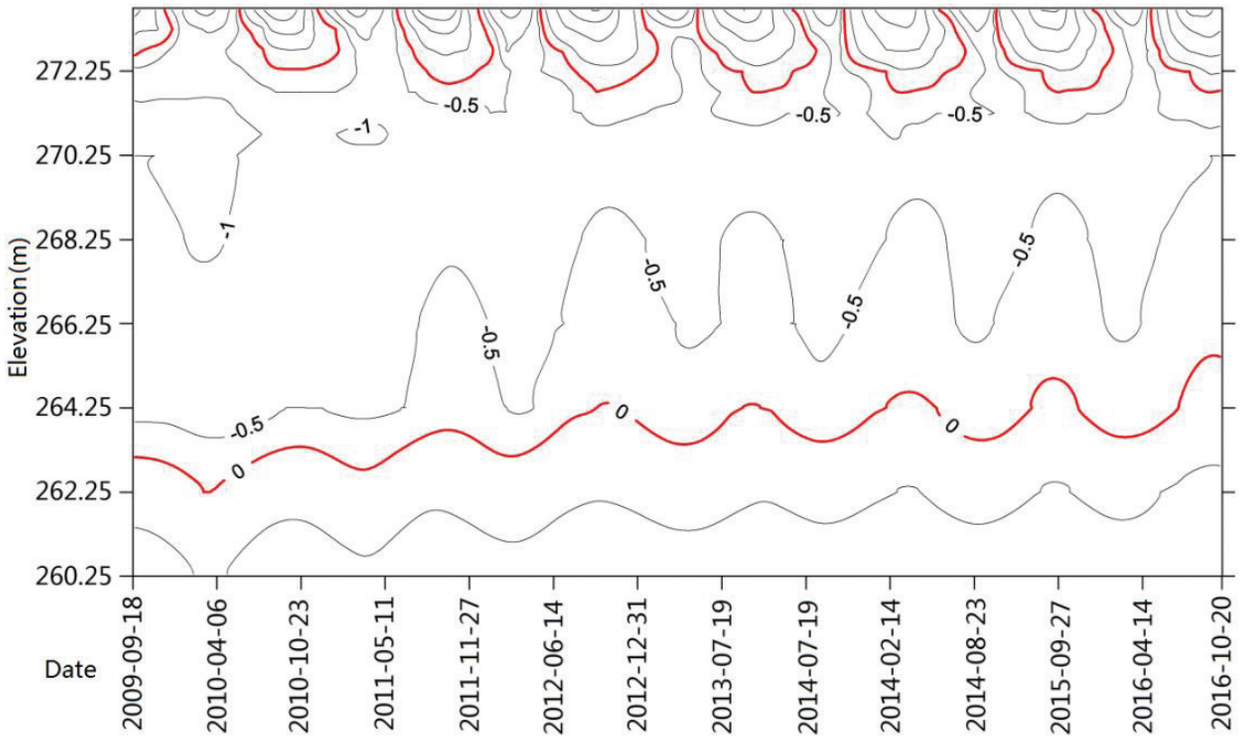

Figure 17. A contour map of ground temperature at T1 (the 0°C isothermal indicates the upper and lower limits of the permafrost).

(**Figure 17**). Seasonally frozen soil and permafrost at T1 were linked together on May 5 each year. On May 5, 2010, the lower limit of the permafrost was 262.4 m; on September 25, 2010, the upper limit of the permafrost was 272.3 m, the lower limit was 263.4 m, the thickness was 8.9 m, and the minimum temperature was −1.0°C. On May 5, 2011, the lower limit of the permafrost was 262.9 m; on September 25, 2011, the upper limit of the permafrost was 271.9 m, the lower limit was 263.8 m, the thickness was 8.1 m, and the minimum temperature was −0.9°C. On May 5, 2012, the lower limit of the permafrost was 263.1 m; on September 25, 2012, the upper limit of the permafrost was 271.7 m, the lower limit was 264.2 m, the thickness was 7.5 m, and the minimum temperature was −0.7°C. On May 5, 2013, the lower limit of the permafrost was 263.2 m; on September 25, 2013, the upper limit of the permafrost was 271.7 m, the lower limit was 264.3 m, the thickness was 7.4 m, and the minimum temperature was −0.7°C; on May 5, 2014, the lower limit of the permafrost was 263.3 m; on September 25, 2014, the upper limit of the permafrost was 271.7 m, the lower limit was 264.8 m, the thickness was 6.9 m, and the minimum temperature was −0.6°C. On May 5, 2015, the lower limit of the permafrost was 263.5 m; on September 25, 2015, the upper limit of the permafrost was 271.7 m, the lower limit was 265.4 m, the thickness was 6.3 m, and the minimum temperature was −0.6°C. On May 5, 2016, the lower limit of the permafrost was 263.8 m; on September 25, 2016, the upper limit of the permafrost was 271.7 m, the lower limit was 265.6 m, the thickness was 6.1 m, and the minimum temperature was −0.5°C.

Ground temperature data suggested that road construction affected the permafrost, since the road was near the subgrade at the left slope toe. The upper limit of the permafrost decreased significantly while the lower limit increased significantly during the road construction. Affected

by temperature and permafrost, the rock and soil strata near the upper and lower limits of the permafrost in this position froze and thawed repeatedly. The overall trend was permafrost degradation as a result of changes in climate, characterized by a rise of the permafrost temperature, a decline of the upper limit, a rise of the lower limit, and a decrease in the thickness.

Figure 18 depicts a contour map at T2 showing the variation in ground temperature and depth of the rock and soil strata and the variation of the upper and lower limits of the permafrost at T2 over time. At T2 at the start of the investigation in July 2009, the upper limit of the permafrost was 269.3 m, the lower limit was 263.3 m, and the thickness was 6.0 m. When the ground temperature monitoring was started in September 2009, the upper limit of the permafrost was 269.2 m, the lower limit was 263.7 m, the thickness was 5.5 m, and the lowest temperature of the permafrost was −0.9°C (**Figure 18**). On September 3, 2010, the upper limit of the permafrost was 268.1 m, the lower limit was 264.8 m, the thickness was 3.3 m, and the minimum temperature of the permafrost was −0.6°C. On September 25, 2016, the upper limit of the permafrost was 266.8 m, the lower limit was 265.2 m, the thickness was 1.6 m, and the minimum temperature of the permafrost was −0.4°C. The height of the subgrade fill at T2 reached 10.4 m, which caused an obvious degradation of the permafrost. During the road construction, the upper limit of the permafrost declined, the lower limit rose, and its thickness significantly decreased. Affected by temperature and permafrost, the rock and soil strata near the upper and lower limits of the permafrost in this position froze and thawed repeatedly. Overall, there was a trend of permafrost degradation as a result of changes in climate.

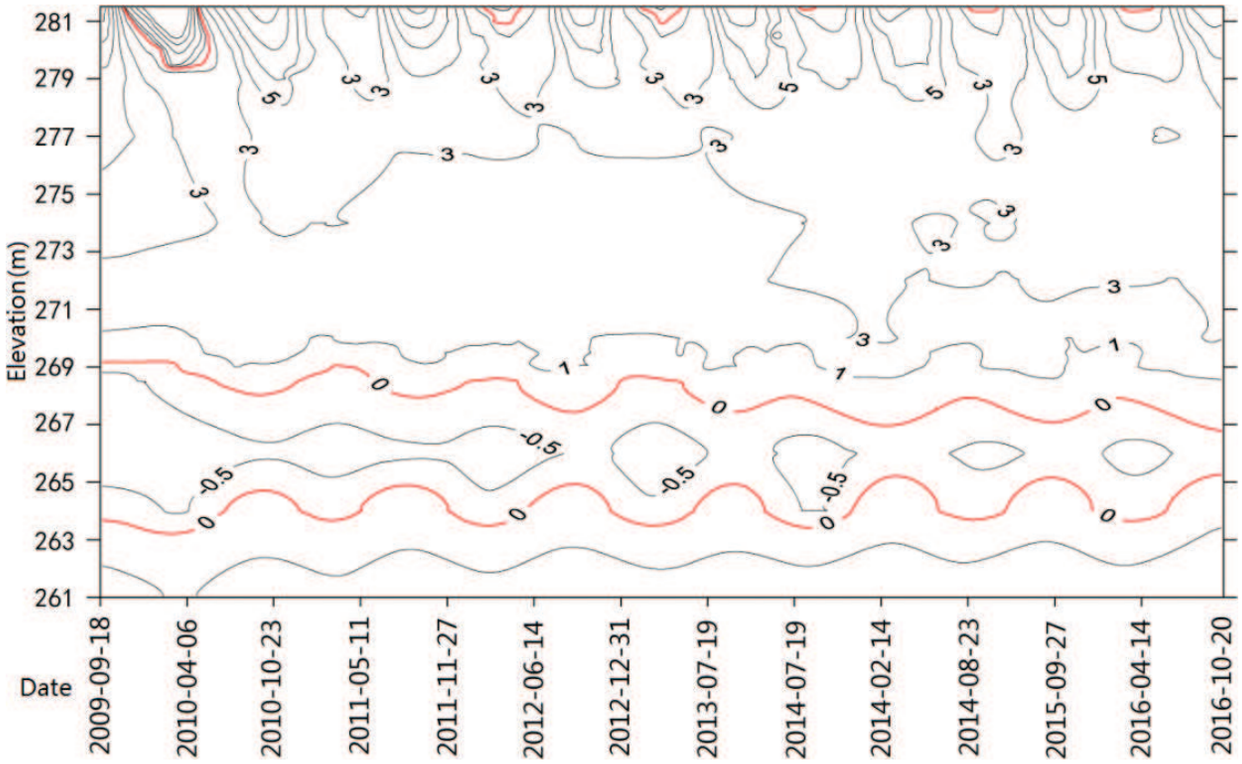

Figure 18. A contour map of ground temperature at T2 (the 0°C isothermal indicates the upper and lower limits of the permafrost).

5.4.2. I–I′ measuring line

Figure 19 shows the HDR inversion image of I–I′ measuring line on September 3, 2010. As indicated by the inversion image, the resistivity stratification of the soil under the measuring line is relatively obvious. To better analyze the variation of soil resistivity with depth, the 2DRES HDR-processing software was used to extract the curve of resistivity at any point on the measuring line. **Figure 20** shows the resistivity curves of the soil at ZK1, ZK2, ZK3, ZK4, and ZK5 as depth changes. According to the resistivity characteristics of the foundation soil on site, soil with resistivity greater than 90 Ωm is probably frozen soil. On September 3, 2010, the upper limit of the frozen soil at ZK1 was 273 m, the lower limit was 263.6 m; the upper limit of the frozen soil at ZK2 was 271.6 m and the lower limit was 264.5 m; the upper limit of

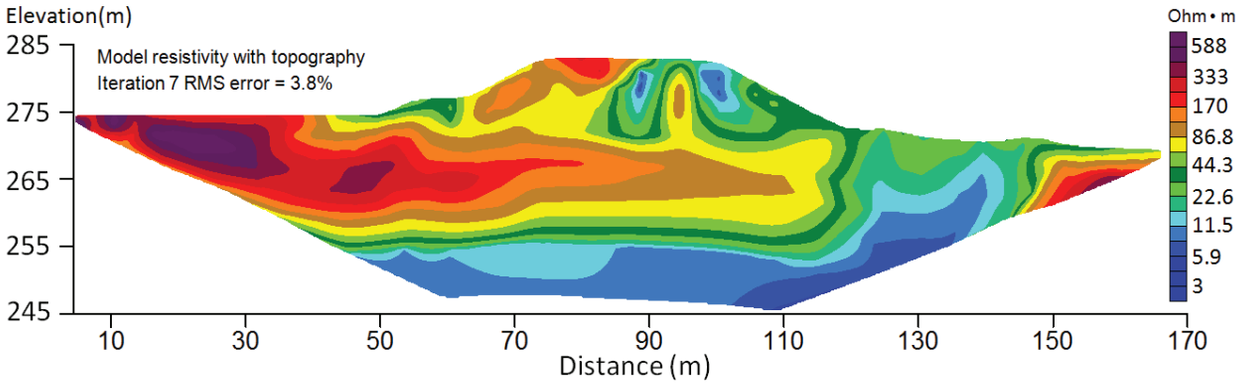

Figure 19. An HDR inversion image of the I–I′ measuring line.

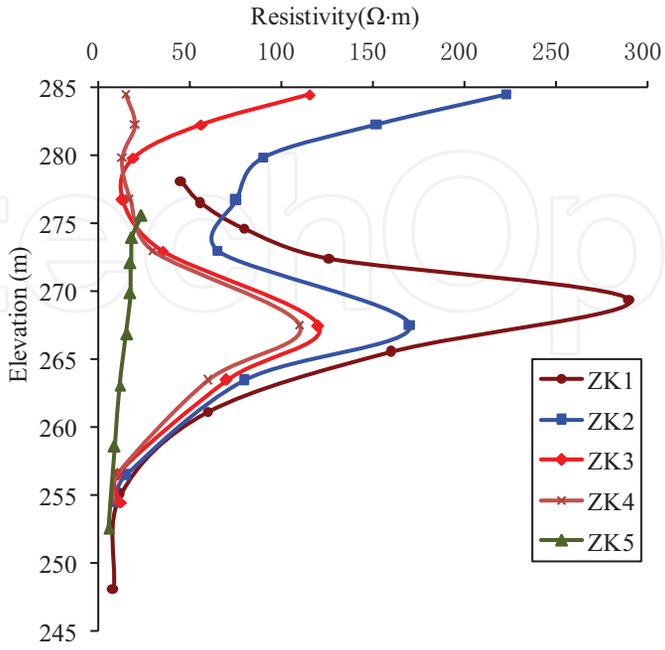

Figure 20. Resistivity curves at different positions of the I–I′ measuring line.

the frozen soil at ZK3 was 269 m and the lower limit was 264.6 m; the upper limit of the frozen soil at ZK4 was 268.3 m and the lower limit was 265.7 m; there was no permafrost at ZK3. The comparison of the temperature-monitoring data at T1 and T2 suggests that there is no difference between the upper and lower limits of permafrost at ZK1 and ZK3, and the position of permafrost inferred by the resistivity data was accurate.

5.4.3. II–II′ measuring line

To explore the variation of permafrost on the II–II′ measuring line, four HDR detection analyses were carried out on the II–II′ measuring line on May 5, 2010, May 5, 2012, May 5, 2014,

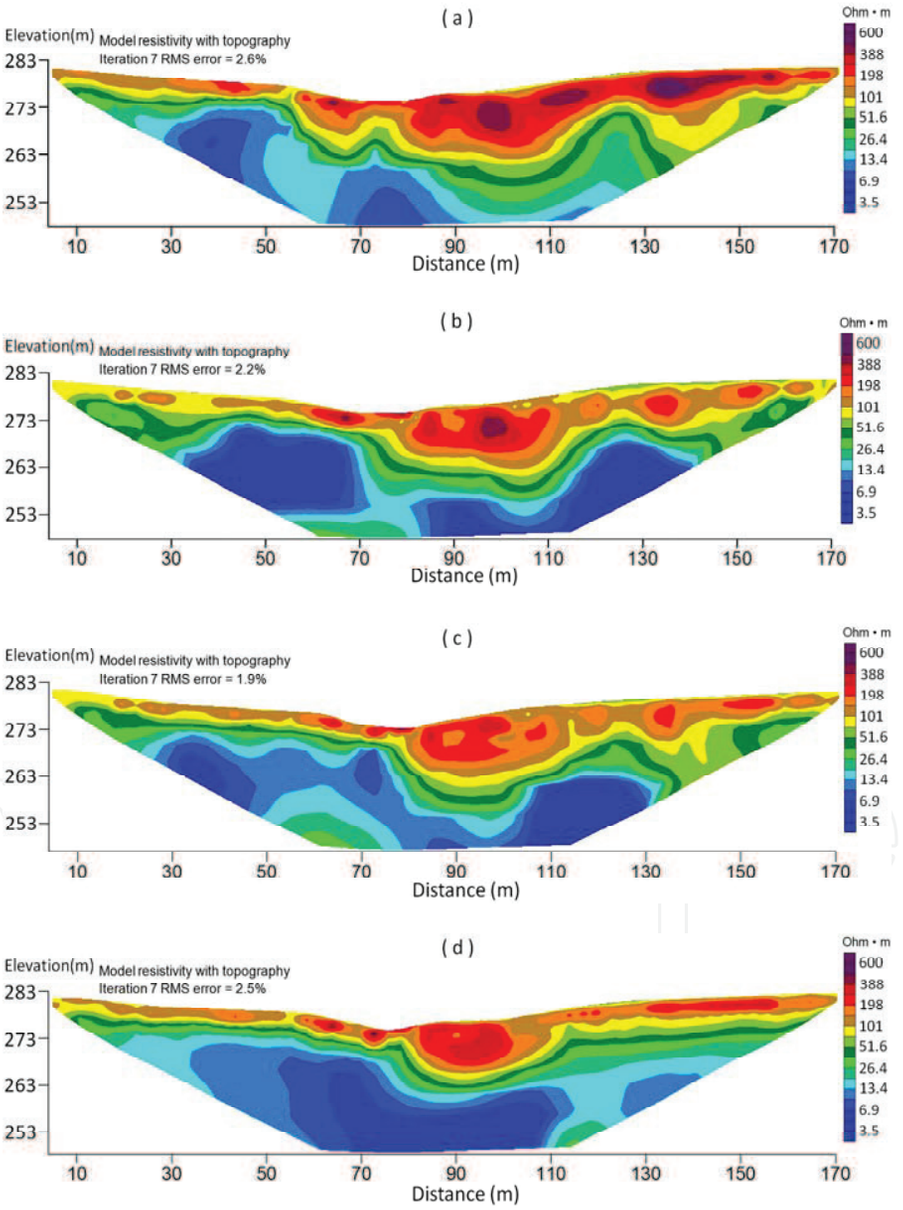

Figure 21. The HDR inversion image of the II–II′ measuring line in May. The measurement dates were May 5, 2010 (a), May 5, 2012 (b), May 5, 2014, (c) and May 5, 2016 (d).

http://dx.doi.org/10.5772/intechopen.68197

and May 5, 2016 (**Figure 21** shows the images gained by these detections). Five HDR detection analyses were carried out on the II–II′ measuring line on September 25, 2010, September 25, 2012, September 25, 2014, September 25, 2015 and September 25, 2016 (**Figure 22** shows the images gained by these detections). ZK1 is a cross section of the K161+440 Road at 90 m from the starting point on II–II′ measuring line.

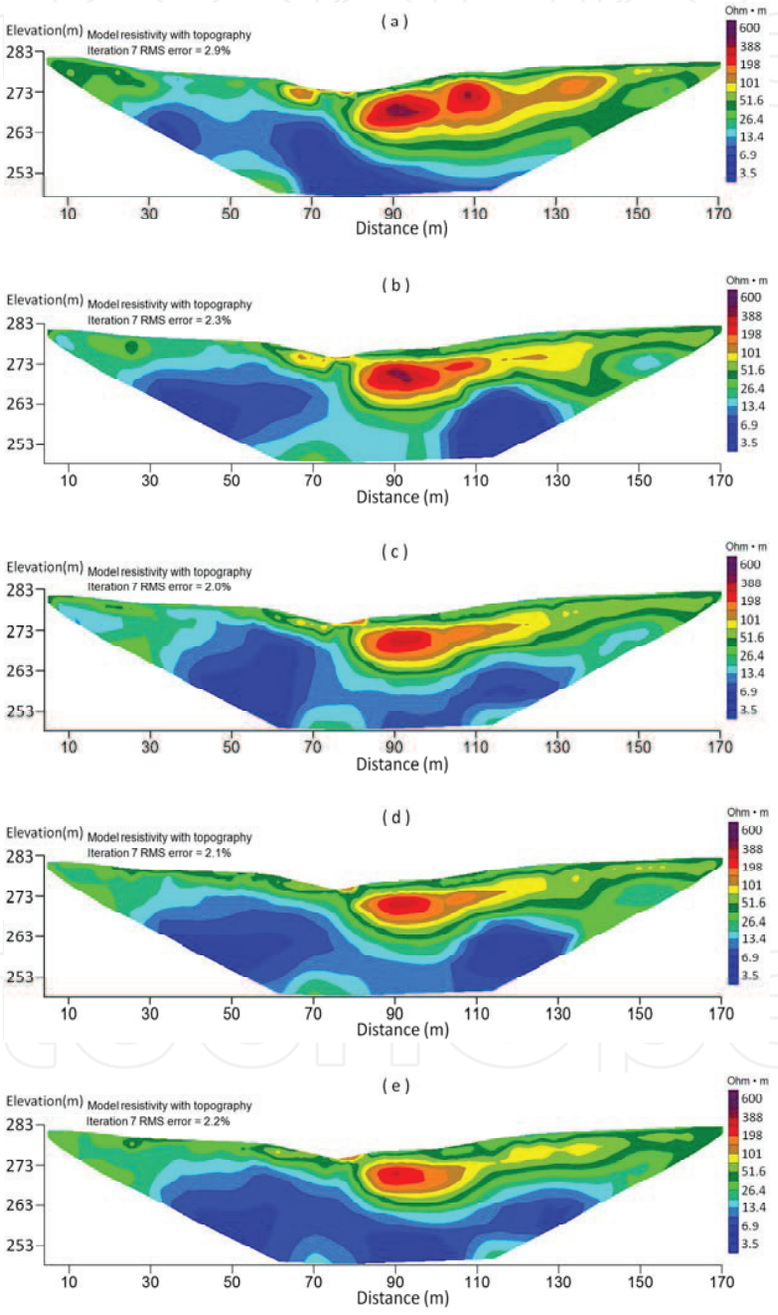

Figure 22. The HDR inversion image of the II–II′ measuring line in September. The measurement dates were September 25, 2010 (a), September 25, 2012 (b), September 25, 2014 (c), September 25, 2015 (d), and September 25, 2016 (e). The surface layer of the K161+424-K161+432 road section (74–82 m away from the starting point) is composed of concrete at the mouth of the culvert and thus this measuring line had a relatively high resistivity.

The lower limits of permafrost at ZK1 were 262.5, 263.0, 263.0, and 264.1 m, respectively, on May 5, 2010, May 5, 2012, May 5, 2014, and May 5, 2016. The upper limits of permafrost at ZK1 were 272.5, 272.0, 272.0, 272.0, and 272.0 m, respectively, on September 25, 2010, September 25, 2012, September 25, 2014, September 25, 2015, and September 25, 2016, with the lower limits being 263.4, 264.0, 264.5, 265.1, and 265.3 m, respectively.

Compared with the lower limit of permafrost obtained by the temperature data at T1, the difference between the upper and lower limits of permafrost measured by the HDR method was small, indicating that the position of permafrost detected by the HDR method on II–II′ measuring line was accurate.

As shown by the measurement results obtained on II–II′ measuring line, both the area and resistivity of the high-resistivity areas were shrinking during the period analyzed, indicating that the permafrost at the left slope toe of the road was constantly degrading. The upper limit of the permafrost was declining, the lower limit was moving up, the temperature was rising, and the total area was decreasing. As shown in **Figure 22**, on II–II′ measuring line, permafrost was found in the following road sections on the following dates: K161+414-K161+422 and K161+431-K161+494 in September 2010; K161+414-K161+422 and K161+431-K161+484 in September 2012; K161+432-K161+477 in September 2014; K161+432-K161+472 in September 2015; and K161+433-K161+460 in September 2016.

5.4.4. III–III′ measuring line

To explore the distribution of permafrost on III–III′ measuring line, HDR detection analyses were conducted on III–III′ measuring line on September 25, 2010 and September 25, 2014 (images are shown in **Figure 23**). ZK5 is a cross section of the K161+440 road at 90 m from the starting

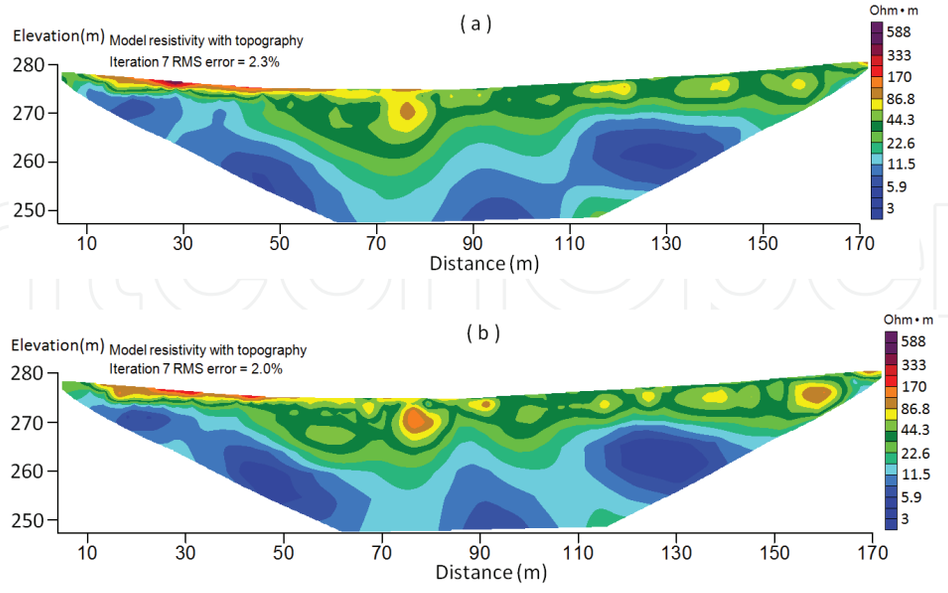

Figure 23. The HDR inversion images of the III–III′ measuring line over time. The measurement dates were September 25, 2010 (a) and September 25, 2014 (b). The surface layer of the K161+424-K161+432 road section (74–82 m away from the starting point) on the measuring line was a culvert within the depth of 0–5 m, thus this line had a relatively high resistivity.

http://dx.doi.org/10.5772/intechopen.68197

point on III–III′ measuring line. The measurement results about the distribution of permafrost in the foundation soil beneath III–III′ measuring line agreed with the drilling results (**Figure 23**).

6. Conclusions

1. The electrical resistivity of the frozen soil was shown to be inversely proportional to the unfrozen water content of the soil body. Temperature determined the exact proportionality. The electrical resistivity of the frozen soil decreased with increases in the unfrozen water content of the soil body. The electrical resistivity of the frozen soil showed a complex temperature-related functional relationship with the initial water content. The electrical resistivity of the frozen soil rapidly decreased at first and then gradually increased with increases in the initial water content of the soil body. The electrical resistivity of the frozen soil tended to stay at the minimum value near the optimum water content. The effect of the dry density on the electrical resistivity of the frozen soil gradually decreased when the initial water content was greater than the optimum water content. The effect of the variation of the water content on the electrical resistivity of the frozen soil increased with decreases in the temperature.
2. The electrical resistivity of the frozen soil was exponentially related to the temperature of the soil body. The electrical resistivity of the frozen soil increased with decreasing temperature. The effect of the temperature of the frozen soil on the electrical resistivity of the frozen soil decreased with increasing water content. When there was a change in the dry density of the frozen soil, the effect of the temperature on the electrical resistivity of the frozen soil was effectively unchanged.
3. The electrical resistivity of the frozen soil was inversely proportional to the dry density of the soil body. The electrical resistivity of the frozen soil decreased with increasing dry density. The effect of the dry density of the frozen soil on the electrical resistivity gradually decreased with increasing water content. The effect of the dry density on the electrical resistivity of the frozen soil increased with decreasing temperature.
4. The relationships between the electrical resistivity of a frozen soil and the various influencing factors were basically consistent with the relationships described by the fitted equations obtained from the experiments, based on the model of the electrical resistivity of frozen soils. This verified the reasonableness of the model for the electrical resistivity of frozen soils. More studies are needed to investigate the related parameters in the model for the electrical resistivity of frozen soils.
5. The results of geological drilling, temperature monitoring, and HDR detection analyses suggest that a widened and expanded subgrade have had a significant influence on permafrost in the K161 road section. During the subgrade construction, the permafrost was degraded as a result of both road construction and climatic change. Permafrost temperatures rose, the upper limit of permafrost declined, the lower limit of permafrost rose, and the overall thickness of the permafrost significantly decreased.
6. The positions of permafrost estimated by the HDR method were in agreement with the results obtained from geological drilling, temperature monitoring, and the electrical

survey, indicating that HDR is a fast, economical, and reliable method for on-site exploration of permafrost. HDR can be used to quickly and accurately locate the position of underground permafrost in high-latitude permafrost regions, providing an accurate reference for linear engineering positioning and corresponding engineering measures.

Acknowledgements

Parts of this chapter are reproduced from authors' recent publication [14, 33]. This project is supported by the Natural Science Foundation of China (Grant No. 41641024).

Author details

Wei Shan*, Zhaoguang Hu, Ying Guo, Chengcheng Zhang and Yao Liu

*Address all correspondence to: shanwei456@163.com

Institute of Cold Regions Science and Engineering, Northeast Forestry University, Harbin, China

References

[1] Wu J, Li CB, Sun HZ. Preliminary observations of the variation of the electrical resistivity of a soil under in-situ conditions. Chinese Journal of Soil Science. 1985:**2**;13 (in Chinese).

[2] Li L, Zhou ZH, Zhang HY. Experimental study on the electrical resistivity of saline soils. Environmental Engineering. 2012;**30**:498–503 (in Chinese with English abstract).

[3] Zha FS, Liu SY, Du YJ, Cui KR. Effect of soil grain composition on soil electrical resistivity. Industrial Construction 2013;**43**(3):71–74 (in Chinese with English abstract).

[4] Fortier R, Allard M, Seguin MK. Effect of physical properties of frozen ground on electrical resistivity logging. Cold Regions Science and Technology. 1994;**22**(4):361–384.

[5] Fortier R, LeBlanc AM, Allard M, Buteau S, Calmels F. Internal structure and conditions of permafrost mounds at Umiujaq in Nunavik, Canada, inferred from field investigation and electrical resistivity tomography. Canadian Journal of Earth Sciences. 2008;**45**(3):367–387.

[6] Delaney AJ, Peapples PR, Arcone SA. Electrical resistivity of frozen and petroleum-contaminated fine-grained soil. Cold Regions Science and Technology. 2001;**32**(2):107–119.

[7] Fu W, Wang R, Hu MJ, Xiang YH. Study of relationship between uniaxial compressive strength and electrical resistivity of frozen soil under different temperatures. Rock and Soil Mechanics. 2009;**30**(1):73–78 (in Chinese with English abstract).

[8] Angelopoulos MC. Integrated geophysical approach for the detection and assessment of ground ice at Parsons Lake, Northwest Territories, Northwest Territories [MSc thesis]. Montreal, Quebec, Canada: McGill University; 2010.

[9] McCann DM, Forster A. Reconnaissance geophysical methods in landslide investigations. Engineering Geology. 1990;**29**:59–78.

[10] Hack R. Geophysics for slope stability. Surveys in Geophysics. 2000;**21**:423–448.

[11] Benedetto A, Benedetto F, Tosti F. GPR applications for geotechnical stability of transportation infrastructures. Nondestructive Testing and Evaluation. 2013;**27**(3):253–262.

[12] Malehmir A, Bastani M, Krawczyk CM, Gurk M, Ismail N, Polom U, Persson L. Geophysical assessment and geotechnical investigation of quick-clay landslides—a Swedish case study. Near Surface Geophysics. 2013;**11**(3):341–350.

[13] Timothy S, Bilderback EL, Quigley MC, Nobes DC, Massey CI. Coseismic landsliding during the Mw 7.1 Darfield (Canterbury) earthquake: Implications for paleoseismic studies of landslides. Geomorphology. 2014;**214**:114–127.

[14] Hu Z, Shan W. Landslide investigations in the northwest section of the lesser Khingan range in China using combined HDR and GPR methods. Bulletin of Engineering Geology and the Environment. 2016;**75**:591–603.

[15] Cardarelli E, Marrone C, Orlando L. Evaluation of tunnel stability using integrated geophysical methods. Journal of Applied Geophysics. 2003;**52**(2–3):93–102.

[16] Yamakawa Y, Kosugi K, Masaoka N, Tada Y, Mizuyama T. Use of a combined penetrometer-moisture probe together with geophysical methods to survey hydrological properties of a natural slope. Vadose Zone Journal. 2010;**9**(3):768–779.

[17] Donohue S, Gavin K, Tolooiyan A. Geophysical and geotechnical assessment of a railway embankment failure. Near Surface Geophysics. 2011;**9**(1):33–44.

[18] Sauvin G, Lecomte I, Bazin S, Hansen L, Vanneste M, LHeureux JS. On the integrated use of geophysics for quick-clay mapping: The Hvittingfoss case study, Norway. Journal of Applied Geophysics. 2014;**106**:1–13.

[19] Carpentier S, Konz M, Fischer R, Anagnostopoulos G, Meusburger K, Schoeck K. Geophysical imaging of shallow subsurface topography and its implication for shallow landslide susceptibility in the Urseren Valley, Switzerland. Journal of Applied Geophysics. 2012;**83**:46–56.

[20] Perrone A, Lapenna V, Piscitelli S. Electrical resistivity tomography technique for landslide investigation: A review. Earth-Science Reviews. 2014;**135**:65–82.

[21] Sass O, Bell R, Glade T. Comparison of GPR, 2D-resistivity and traditional techniques for the subsurface exploration of the Oschingen landslide, Swabian Alb (Germany). Geomorphology. 2008;**93**(1):89–103.

[22] Sass O. Bedrock detection and talus thickness assessment in the European Alps using geophysical methods. Journal of Applied Geophysics. 2007;**62**:254–269.

[23] Schrott L, Sass O. Application of field geophysics in geomorphology: Advances and limitations exemplified by case studies. Geomorphology. 2008;**93**:55–73.

[24] Zajc M, Pogacnik Z, Gosar A. Ground penetrating radar and structural geological mapping investigation of karst and tectonic features in flyschoid rocks as geological hazard for exploitation. International Journal of Rock Mechanics and Mining Sciences. 2014;**67**:78–87.

[25] Havenith HB, Jongmans D, Abdrakhmatov K, Trefois P, Delvaux D, Torgoev A. Geophysical investigations of seismically induced surface effects: Case study of a landslide in the Suusamyr valley, Kyrgyzstan. Surveys in Geophysics. 2000;**21**:349–369.

[26] Bichler A, Bobrowsky P, Best M, Douma M, Hunter J, Calvert T, Burns R. Three-dimensional mapping of a landslide using a multi-geophysical approach: The Quesnel Forks landslide. Landslides. 2004;**1**(1):29–40.

[27] Drahor MG, Gokturkler G, Berge MA, Kurtulmus TO. Application of electrical resistivity tomography technique for investigation of landslides: a case from Turkey. Environmental Geology. 2006;**50**(2):147–155.

[28] Rhim CH. Measurements of dielectric constants of soil to develop a landslide prediction system. Smart Structures and Systems. 2011;**7**(4):319–328.

[29] Shan W, Hu Z, Guo Y, Zhang C, Wang C, Jiang H, Liu Y, Xiao J. The impact of climate change on landslides in southeastern of high-latitude permafrost regions of china. Frontiers in Earth Science. 2015;**3**(7):1–11.

[30] Archie GE. The electrical resistivity log as an aid in determining some reservoir characteristics. Transactions of American Institute of Mining Engineers. 1942;**146**(1):54–61.

[31] Waxman MH, Smits LJM. Electrical conductivities in oil-bearing shaly sands. Society of Petroleum Engineers Journal. 1968;**8**(2):107–122.

[32] Zha FS, Liu SY, Du YJ. Study on the electrical resistivity characterization of unsaturated clay. Geotechnical Investigation & Surveying. 2006;**7**:1–4 (in Chinese with English abstract).

[33] Wei S, Yao L, Zhaoguang H, Jitao X. A model for the electrical resistivity of frozen soils and an experimental verification of the model. Cold Regions Science and Technology. 2015;**119**:75–83.

[34] Topp GC, Davis JL, Annan AP. Electromagnetic determination of soil water content: Measurements in coaxial transmission lines. Water Resources Research. 1980;**16**(3): 574–582.

[35] Li L. Study on the characteristics of the electrical resistivity of saline soils [Master's thesis]. Lanzhou, China: Lanzhou University; 2012.